Co FeO @rGO composite: Towards trifunctional water splitting in alkaline media

Abdul Hanan, Dong Shu, Umair Aftab, Dianxue Cao, Abdul Jaleel Laghari, Muhammad Yameen Solangi, Muhammad Ishaque Abro, Ayman Nafady, B. Vigolo, Aneela Tahira, et al.

Co_2FeO_4@rGO composite: Towards trifunctional water splitting in alkaline media

Abdul Hanan[a], Dong Shu[a], Umair Aftab[b], Dianxue Cao[a*], Abdul Jaleel Laghari[b], Muhammad Yameen Solangi[b], Muhammad Ishaque Abro[b], Ayman Nafady[e], Brigitte Vigolo[d], Aneela Tahira[c], Zafar Hussain Ibupoto[c]*

[a]Key Laboratory of Superlight Material and Surface Technology, Ministry of Education, College of Materials Science and Chemical Engineering, Harbin Engineering University, PR China.

[b]Department of Metallurgy and Materials Engineering, Mehran University of Engineering and Technology, 76080, jamshoro, Pakistan.

[c]Dr. M.A Kazi Institute of Chemistry University of Sindh Jamshoro, 76080, Sindh Pakistan

[d]Université de Lorraine, CNRS, IJL, F-54000 Nancy, France

[e]Department of Chemistry, College of Science, King Saud University, Riyadh 11451, Saudi Arabia

*Corresponding authors: Dianxue Cao and Zafar Hussain Ibupoto

Email : caodianxue@hrbeu.edu.cn zaffar.ibhupoto@usindh.edu.pk

Abstract

Development of efficient, low cost and multifunctional electrocatalysts towards water splitting to harvest hydrogen fuels is a challenging task, but the combination of carbon materials with

transition metal-based compounds is providing unique and attractive strategy. Herein, composite systems based on cobalt ferrite oxide (Co_2FeO_4) @reduced graphene oxide (rGO) using simultaneous hydrothermal and chemical reduction method have been prepared. The proposed study eliminates one step of conversion of GO into rGO and it uses direct GO during the synthesis of cobalt ferrite oxide, consequently rGO based hybrid system is achieved with less labor and economy. The optimized composite has revealed an outstanding multifunctional application towards water splitting reactions such as oxygen reduction reaction (ORR), oxygen evolution reaction (OER) and hydrogen evolution reaction (HER). Various metal oxidation states and oxygen vacancies at the surface of Co_2FeO_4@rGO composites guided the multifunctional surface properties. The optimized Co_2FeO_4@ rGO composite presents excellent multifunctional properties with onset potential of 0.60 V for ORR, and an overpotential of 240 mV and 320 mV at a 20 $mAcm^{-2}$ for OER and HER respectively. The outstanding multifunctionalities of the optimized Co_2FeO_4@ rGO composite are associated to high electrical conductivity, high density of active sites, crystal defects, oxygen vacancies, and favorable electronic structure with the substitution of Fe for Co atoms in binary spinel oxide phase. These surface features synergistically uplifted the electrocatalytic properties of Co_2FeO_4@rGO composites. The multifunctional properties of the Co_2FeO_4@ rGO composite could be of high interest for its use in wide range of applications in sustainable and renewable energy fields.

Keywords: Reduced graphene oxide(rGO), bimetallic cobalt iron ferrite, composite systems, multifunctional electrocatalysts

Graphical Abstract: Illustration of multifunctional surface properties of Co_2FeO_4@rGO composite

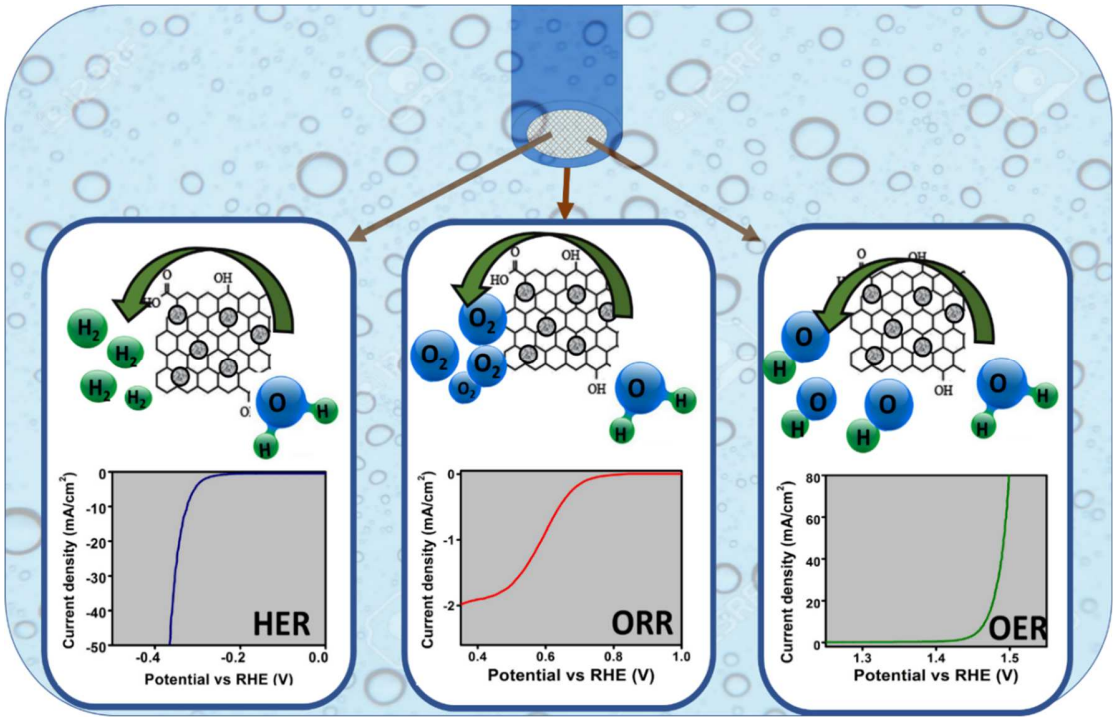

1. Introduction

Energy crisis and environmental pollution challenges require the development of outperforming energy conversion and storage devices [1, 2]. Water splitting for H2 production is an appealing solution. Water splitting is able to transform solar energy for the generation of H2 [3-7]. It is well established that the dynamic efficiency of oxygen reduction reaction (ORR), oxygen evolution reaction (OER) and hydrogen evolution reaction (HER) is crucial for the development of high performance metal air batteries, overall water splitting and hydrogen generation [8, 9, 10, 11]. The current challenge towards efficient water splitting is the immediate need of having outperforming nonprecious electrocatalysts. However, currently available electrocatalysts in the market are platinum (Pt) for the oxygen reduction reaction (ORR) as cathode in batteries, hydrogen evolution reaction (HER) as cathode and oxygen evolution reaction (OER) as anode in water electrolyzer, creating an economic issue due to their expensive nature [12]. To date, Pt and IrO_2/RuO_2 supported carbon are the-state-of-art electrocatalysts towards HER/ORR and OER, respectively.

The high cost and scarcity of Pt, Ir, Ru-based electrocatalysts for HER, ORR and OER create an economic stress, in addition to their poor electrochemical stability, therefore these obvious issues limit the large scale applications of precious electrocatalysts for water splitting [13]. Moreover, Pt/C could produce corrosion and decrease the physical force between the carbon support and Pt nanoparticles, which creates an aggregation of Pt nanoparticles and detachment from the carbon material. These are the worst aspects of using precious Pt/C electrocatalyst and its limitations towards large scale fuel cell commercialization [14]. This is the main reason to develop catalytic materials either with low content of Pt or completely Pt-free nonprecious catalysts to uplift the fuel cell technology [15]. Since two decades, noble metal-free electrocatalysts based on 3-d transition metals like (Fe, Co, Ni and Mo) and their oxides, sulfides, carbides, nitrides, phosphides and alloys have been investigated for simultaneous water splitting applications such as OER, ORR and HER due to their production from abundance resources, low cost and significant catalytic activity [16-21]. Additionally, these metal oxides have negligible aggregation during electrochemical testing in comparison to platinum or its compounds, therefore they are very favorable for the fuel cell technology [22]. The interfacial chemistry and density of catalytic sites of transition metal oxides can be enhanced via using substrates with high specific surface. The enhancement in the interfacial properties, high density of active sites and high surface to volume ratio are the demanding pillars towards the development of commercial fuel cells [23, 24], lithium ion battery [25], and

supercapacitors [26]. The binary spinel compounds have shown excellent catalytic activity [27, 28]. The use of Fe substituent in the binary spinel compounds has demonstrated an auxiliary and crucial role in improving the durability [29].

Among the binary spinel compounds, cobalt ferrite oxide exhibits a wide range of applications such as actuators, stress sensors, actuators, memory storage and magnetoelectric microwave devices and its magnetic properties are approximately equal to that of $Y_3Fe_5O_{12}$ ferrite [30, 31]. Cobalt ferrite oxide owing to its spinel structure offers plenty of attractive physical and chemical features. The spinel structure of cobalt ferrite oxide is carrying mixed oxidation states of A^{2+}/A^{3+}, and they further accelerate the kinetics of electrochemical reactions [32, 33]. It has been shown that the electronic structure of $Co^{3+}{}_{Oct}$ in form of spinel Co_3O_4 could be tuned by addition of $Fe^{3+}{}_{Oct/Td}$. The replacement of Co atoms by Fe could induce the change in Co-O bond length and consequently effect on covalent character of bond [34].

Furthermore, the functionality, electrical conductivity, surface to volume ratio and stability of transition metal oxides could be highly increased through the addition of carbon based materials due to synergetic effect [35]. Wang et al. reported the bimetallic oxide of cobalt-iron (Co2FeO4) supported on multiwall carbon nanotubes as an electrocatalyst towards ORR process [36]. The conductive graphene oxide (GO) is a low cost carbon material and has promising potential towards lifting of catalytic properties [37]. Further reduction of GO into reduced graphene oxide (rGO) has higher electrical conductivity and it can have large possibility to enhance the surface area of metal oxides, thereby increase in current density and superfast charge transport is achievable [38]. In the rGO, the presence of π network is confirming the typical features of graphene [39, 40, 41]. The existing literature reveals that there are no reports on the cobalt ferrite oxide as multifunctional electrocatalyst towards three core HER, OER and ORR reactions. Also, there is no composite system of Co_2FeO_4@rGO prepared by simultaneous reduction and hydrothermal method and its investigation as multifunctional electrocatalyst performing at the same time for HER, OER and ORR reactions. Furthermore, the variation in metal oxidation states and oxygen vacancies at the surface of Co_2FeO_4@rGO composites together for the multifunctional electrochemical properties are not reported. To date

In this study, we have prepared hybrid Co_2FeO_4@rGO systems by simultaneous hydrothermal and reduction method. The Co_2FeO_4@rGO composite is characterized by a variety of analytical

techniques in terms of structure, composition, morphology, crystalline features, surface properties, stability and durability. The optimized Co_2FeO_4@rGO composite has revealed multifunctional proprieties towards HER, OER and ORR reactions with pronounced performance.

2. Experimental work

2.1. Chemicals used:

Graphite, sodium Nitrate ($NaNO_3$), potassium permanganate ($KMnO_4$), hydrogen peroxide (H_2O_2), sulfuric acid (H_2SO_4), hydrochloric acid (HCl), cobalt chloride hexahydrate ($CoCl_2$. $6H_2O$), iron chloride hexahydrate ($FeCl_3.6H_2O$), polyethylene glycol (PEG), 20%Pt/C, 20%RuO_2/C, potassium hydroxide (KOH) and hydrazine hydrate (N_2H_4). The chemicals were purchased from Sigma Aldrich, Karachi Pakistan. All the chemicals were of analytical grade and used without pretreatment. The precursors solutions were prepared in the deionized water.

2.2. Synthesis of Co_2FeO_4@rGO composite nanostructures by simultaneous hydrothermal and reduction method

Desired nanostructures were synthesized by two steps. Initially graphene oxide (GO) was synthesized by modified Hummers method by taking 2 g of graphite flakes and $NaNo_3$ into H_2SO_4 in volumetric flask (1000 mL) under continuous stirring at approximately -5 ℃ in ice bath. After the continuous stirring for 2 hours, 6 g of potassium permanganate was added carefully under the controlled conditions of temperature below 15 ℃. Then, ice bath was removed and the resultant solution was stirred at 35 ℃ for 48 h to get brownish paste like material. Then, 100 mL of deionized water was added into it slowly. The reaction temperature was increased quickly up to 98 ℃ and a brown color for the material was obtained. Furthermore, the solution was diluted with 200 mL of water under continuous stirring. The obtained solution was treated with 10 mL of H_2O_2 to terminate the mechanism to get a yellow color, then mixture was collected and washed with 10% of HCl and deionized water several times, and collected by centrifugation. Afterwards, the filtration and drying was performed under vacuum at room temperature, then a final product of GO powder was obtained [42, 43]. Secondly, 1M PEG, 0.02M cobalt chloride hexahydrate and 0.01M iron chloride were added into the deionized water and kept at magnetic stirring to get well dissolved precursor solution. Then, 1 mL of hydrazine was added drop wise into the solution under constant stirring at room temperature. Hydrazine is as reducing agent to induce GO to rGO transition and stabilizing

agent for the nanostructured materials. Later on, rGO was added with varying concentrations from 5 mg to 10 mg into the solution. The final solution was transferred into 100 mL Teflon autoclave with capacity of 70 mL and heated at 180°c for 5 hours in an electric oven. After the hydrothermal chemical reaction, as received precipitates were washed several times with the deionized water followed by ethanol. Eventually, the product was dried at 80°C in air overnight. Furthermore, the obtained product was treated at 500°C for two hours in air to get cobalt ferrite oxide@rGO as final product. The prepared Co_2FeO_4@rGO composites with different quantities of 5 and 10 mg of rGO are referred to as CFG-5 and CFG-10. The pristine cobalt ferrite oxide sample was prepared via hydrothermal process without the addition of GO.

2.3.Physical characterization of different Co_2FeO_4@rGO composite materials

The morphology of as prepared nanomaterials was studied through scanning electron microscopy (SEM) by JEOL JSM-6480A with operating voltage of 20kV. The energy dispersive spectroscopy (EDS) was applied to determine sample composition. Crystallographic study was carried out through X-ray diffraction (XRD) by using Rigaku TTR at 40 kV with high(?) intensity Cu-Kα radiation (λ=0.15406 nm). Transmission electron microscopy (TEM) using a FEI Tecnai G2 (containing a Schottky emitter functioning at 200kV) was applied for further detailed studies of morphology. Chemical attachment of various elements was observed by X-ray photoelectron spectroscopy (XPS) by using PerkinElmer PHI 5100 XPS X-ray Photoelectron Spectrometer System. Curve fitting was performed using a combined Gaussian and Lorentzian line profile after Shirley's background subtraction by Casa XPS software. To analyze the chemical structure, the Raman spectroscopy was applied by using PerkinElmer RamanStation 400. Fourier transform infrared (FTIR) spectroscopy was applied (PerkinElmer Spectrum 2) on samples having shape of pellets to get information on the functional groups of various electrocatalysts in the region 4000 to 400 cm^{-1}. The UV-Vis spectroscopy by Lambda-365 was used to analyze absorbance of different nanocomposites which were dispersed in deionized water. X-ray photoelectron spectroscopy spectra were collected on a Kratos Axis Ultra (Kratos Analytical, UK) spectrometer equipped with a monochromatic Al Kα (1486.6 eV). All spectra were recorded at a 90° takeoff angle. The high-resolution regions were acquired with 0.1 eV step and 20 eV pass energy (instrumental resolution better than 0.5 eV). Curve fitting was performed using a combined Gaussian and Lorentzian line profile after Shirley's background subtraction by Casa XPS software.

2.4. Electrochemical measurements of Co_2FeO_4@rGO composite materials

Different Electrochemical tests were carried out through an electrochemical workstation (Potentiostat VersaSTAT-4) equipped with a computer. For HER, OER and ORR all the experiments were done on three electrodes electrochemical system into 1.0 M KOH solution. Silver-silver chloride and graphite rod was used as reference electrode and counter electrode and modified glassy carbon electrode (GCE) was used as working electrode. To prepare catalyst ink for electrochemical tests, 5 mg of each catalyst material was added into 1 mL of deionized water and 0.5 ml of 5% Nafion as binder was added into the solution. The obtained catalyst solution was dispersed for 10 minutes in an ultrasonic bath. Later, 5µL of ink was coated on GCE by drop casting method and dried at room temperature. The loading mass of each catalyst was about 0.2 mg/cm^2. The catalytic activity towards HER and OER was studied through linear sweep voltammetry (LSV), under the potential window from 0 to -1.5V and 0 to 0.7 V at scan rate of 5 mV/s respectively. For ORR we have applied LSV at static conditions first, in the potential range from 0 to -1.2 V at various scan rates (5, 20, 40, 60, 80, 100 and 120 mV/sec). Secondly, ORR tests were carried by varying the rotation speed (0, 20, 40, 60, 80 rounds per minute, RPM) under fixed scan rate of 5 mV/sec. This RPM mechanism has been done through rotating assembly in1.0 M KOH solution by magnetic stirring with fixed position of counter, reference and modified glassy carbon electrode. Electrochemical impedance spectroscopy (EIS) was done with sinusoidal potential of 10 mV and onset potential of 1.4 V versus reversible hydrogen electrode (RHE) at frequency range of 100 kHz to 0.1Hz. Chronopotentiometry was applied to investigate the durability of optimized composite system during OER and HER performance at 20, 40 and 60 mA/cm^2 and 10, 20 and 30 mA/cm^2 for 48 hours, respectively. The stability was studied before and after durability test through LSV technique. The double layer capacitance (C_{dl}) was calculated from CV curves in the voltage range from 0.05V to 0.25V at various scan rates (30, 50, 70, 90, 110 and 130 mV/s). Through Nernst equation, all given potentials are reported in this manuscript against RHE. The experimental part is briefly described in Supplementary scheme 1.

3. Results and Discussion

3.1. Morphology, crystalline structure, and chemical composition of various Co_2FeO_4@rGO nanostructured materials

The in situ transformation of GO into rGO during the cobalt ferrite synthesis has resulted a hybrid system which played a significant role in driving the water splitting at low energy consumption.

The XRD patterns of pristine GO, Co_2FeO_4 and various Co_2FeO_4@GO composite materials are shown in Fig. 1. The diffraction patterns at 12.2° and 42.8° are correspond to (001) and (100) crystal planes respectively and these patterns demonstrate the typical characteristics of pristine GO [44]. There is some noisy background form 15-40o indicates the incomplete oxidation of graphite into GO, thus it is presented in the pristine GO sample. While, the pristine Co_2FeO_4 has various diffraction peaks at 19.1°, 31.3°, 36.7°, 44.9°, 59.5° and 65.1° assigned to (111), (220), (311), (400), (511), (440) crystal planes and they are fully agreed to reported work [36]. The addition of GO with different quantities during the synthesis of Co_2FeO_4@GO composites brought substantial changes in the XRD patterns and intensities of reflections which is still unclear to us to identify in this study. It has been found the reflection of GO at (100) crystal plane was disappeared in the composites due to high probability of formation of thick layer Co_2FeO_4 crystalline on GO [45]. We have used a very small amount of GO in the hybrid system, whereas XRD measurement has mainly revealed the patterns of cobalt ferrite. However, XRD results have shown a minor shift in two theta angle towards low angle with the addition of GO and possibly it could create the defects in the composite material resulting to favorable catalytic activity. An addition of GO has also decreased the intensity of some of the cobalt ferrite oxide reflections during the composite formation and no another impurity was found during the XRD analysis.

Initially, the morphological features of pristine Co_2FeO_4, GO and Co_2FeO_4@rGO composites were analyzed through SEM equipped with EDS for the quantification of main elements. As clearly observed in Fig. 2(a), GO has exhibited a nanosheets like structure. The EDS spectrum of GO has confirmed the presence of C and O elements as shown in right side of Fig. 2(a). Co_2FeO_4 has revealed sphere like architecture as shown in Fig. 2(b). The EDS study has verified the presence of Co, Fe and O as main elements as shown in Fig. 2(b) and the obtained elemental information was found consistent with the published work [46]. The microflakes of GO are covered with oxide nanoparticles and remained underneath of cobalt ferrite oxide layer in the case of composite systems of CFG-5 and CFG-10 as shown in Fig. 2(c and d).

The Co_2FeO_4@rGO composite system of CFG-5 has shown some irregular shape, whereas CFG-10 composite has shown highly intense nanoflakes like structure which could be attributed to excessive amount of GO. The presence of Fe, Co, O and C elements was quantified from Co_2FeO_4@rGO composites through EDS analysis. The Co_2FeO_4@rGO composites revealed a better surface features like small particle size in comparison to pristine GO and Co_2FeO_4 materials, thus they have shown better electrochemical properties. An addition of higher quantity of GO resulted in more carbon during the hydrothermal process as confirmed by EDS in terms of carbon content, which is further giving an idea of enhanced conductivity and large surface for the swift interaction of water molecules during electrolysis.

The HRTEM images and fast Fourier transform (FFT) patterns have been recorded to analyze the fine structure of various nanostructures at atomic level. Fig 3a shows HRTEM image of pristine Co_2FeO_4 which reveals well dispersed nanoparticles with different shapes and the corresponding FFT image is displayed at right side indicating the lattice fringes with d-spacing of 0.23 nm. Fig. 3b shows the nanosheets of graphene oxide and its FFT image, describing the typical d-spacing of 0.20 nm of graphene. The Co_2FeO_4@rGO composites (Fig. 3c and d), characterized with slight folding at the edges correlated to reduced graphene oxide layers. The FFT images of both Co_2FeO_4@rGO composites exhibited the lattice fringes with d-spacing of 0.24 nm and 0.25 nm for CFG-5 and CFG-10 composites, respectively. The presence of plenty edges in the Co_2FeO_4@rGO composites are providing significant catalytic sites for the water catalysis. The lattice fringes of the composite systems are comparable to those of pristine rGO and cobalt ferrite oxide, suggesting a high possibility of chemical coupling between GO and cobalt ferrite oxide The strong chemical coupling is further enhancing the hybrid material stability and reproducibility during the electrochemical characterization.

The chemical composition and the valence state of GO, Co_2FeO_4, CFG-5 and CFG-10 were investigated by XPS. The corresponding XPS survey scans show that the prepared samples including the hybrid nanomaterials are of high purity (Figure S1 a). C1s features show that GO is in a reduced form in the Co_2FeO_4@rGO composites since the contributions related to the carbon-oxygen bonds are diminished compared to GO (Figure S1 b). Figure shows O1s, Fe2p and Co2p XPS features of CFG-5 and CFG-10. The O1s peak was de-convoluted into two peaks positioned at 530.2-530.3 (O_I) and 531.4-531.6 eV (O_{II}), corresponding to the stoichiometric oxidized metal-

oxygen bonds and oxygen vacancies, respectively [47]. The O_{II} area proportion ($O_{II}/(O_{II}+O_I)$) represents the relative quantity of oxygen vacancy. CFG-5 and CFG-10 exhibit 53 and 51 % of oxygen vacancies, respectively. Fe 2p3/2 was deconvoluted into Fe^{2+} (710.60-710.70 eV) and Fe^{3+} (712.5-713.00 eV) peaks [48] as shown in Figures 4c and 4d. Fe^{2+}/Fe^{3+} ratio is calculated to be 0.23 and 0.62 for CFG-5 and CFG-10, respectively. Co 2p3/2 doublet was well fitted by the tetrahedral Co^{3+} (780 eV) and octahedral Co^{2+} (781.3 eV) contributions [49, 50]. Co^{3+}/Co^{2+} ratio is found to be ~ 0.44 and 0.70 for CFG-5 and CFG-10, respectively. The XPS analysis has confirmed the higher concentrations of Fe^{2+} in CFG-5, Co^{3+}in CFG-10 and oxygen vacancies in CFG-5, suggesting that an addition of GO has dominant role in altering the metal oxidation states and oxygen vacancies at the surface of Co_2FeO_4@rGO composites, further driving the multifunctional surface properties.

The Raman spectroscopy has been applied on various nanostructures to analyze their band states. As shown in supplementary Fig. S2(a), three corresponding peaks have been analyzed, the D band at 1353 cm^{-1}, G band at 1580 cm^{-1} and the 2D band at around 2705 cm^{-1} in the Raman spectrum of carbon atoms in graphene oxide sheets. The G band corresponds to sp_2 hybridization of carbon atoms, the D band is commonly related to sp^3 carbon defects [51, 52]. As for Co_2FeO_4, all the relevant bands can be clearly observed at 298 cm^{-1}, 476 cm^{-1} and 680 cm^{-1} which correspond to the presence of Co, Fe and O elements as depicted in supplementary Fig. S2(b) [53]. The Raman shifts for the Co_2FeO_4@rGO composites exhibit slight changes in the corresponding band intensity as shown in supplementary Fig. S2(c). Interestingly, the addition of graphene oxide has decreased intensity of D band and slight enhancement of G band is observed. As expected an addition of hydrazine in precursor of cobalt ferrite oxide resulted to the reduction of GO into rGO as confirmed from decrease in the intensity of D band [54]. Raman and XPS results have successfully verified that we have achieved the in-situ growth of cobalt iron ferrite and rGO composite in the single step. The Raman spectroscopy analysis has shown strong interaction between GO and Co_2FeO_4 in terms of band position and enhancement of G band intensity, indicating another evidence for strong chemical coupling of GO with cobalt ferrite oxide in the hybrid system. The Raman study is supporting the observations made on the electrochemical reactions related to the enhanced conductivity and multifunctional properties.

The FTIR analysis was performed to identify the functional groups within pristine GO, Co_2FeO_4 and Co_2FeO_4@rGO composites. Generally, the absorption bands of O-H, C-H, C=O, O-H, C-O

and C=C groups were located at 3440, 2930, 1790, 1025, and 873 cm^{-1}, respectively as depicted in supplementary Fig. S2(a). The metal oxide (M-O) absorption bands were seen at 650 and 590 cm^{-1} which further suggest the presence of typical metal oxide bonds like Co-O and Fe-O bonds [55]. As shown in supplementary, the broader absorption bands are shown due to nanostructure phase of cobalt ferrite oxide. Moreover, the addition of GO has made significant change in stretching vibration bands of pristine Co_2FeO_4 sample in the hybrid system, which could be related to the interaction between binary metal oxide and GO as shown in supplementary Figure S3 (a). Furthermore, the UV-visible absorption study was carried on various nanostructures to confirm optical features of as prepared materials. As shown in Fig. S3(b), the absorption peak of pristine Co_2FeO_4 observed at 280 nm which corresponds to Co-O existence within the composite [56, 57]. The pristine GO has absorbance peak at 232 nm which corresponds to π-π^* transition of remaining sp^2 C=C bonds. However, as prepared Co_2FeO_4@rGO composites including CFG-5 and CFG-10 have shown slight change in the absorption intensity at 232 nm compare to pure Co_2FeO_4.

3.2.**Multifunctional perspectives of Co2FeO4@rGO composite as an electrocatalyst**

The multifunctional properties of in situ produced Co_2FeO_4@rGO composites and their pristine components were studied toward ORR, OER and HER characterization.

It has been identified that ORR as a backbone reaction of fuel cells and metal-air batteries [58, 59]. For this purpose, we tested the different as prepared nanostructures including pristine GO, Co_2FeO_4, composite Co_2FeO_4@rGO materials and 20%Pt/C. The evaluation of ORR functionality of these materials in terms of half wave potential was studied by linear sweep voltammetry in oxygenated 1.0 M KOH aqueous solution in a potential window of 0.2 to 1.12 at sweeping rate of 5 mVs^{-1} as shown in Fig. 5(a). The corresponding half wave potential values of 0.59, 0.58, 0.56 and 0.60 V were observed for pristine GO, and Co_2FeO_4, and Co_2FeO_4@rGO composites including CFG-5 and CFG-10 respectively and in comparison to the state-of-art Pt/C catalyst with half wave potential of 0.85 V as shown in Fig. 5(b). The obtained results confirm that the Co_2FeO_4@rGO composite like CFG-10 has superior ORR activity as compared with previous reported research work as shown in Table (S3). The corresponding K-L plots of CFG-10 are depicted in Fig. 5(c). Note that the great linearity along with consistent slope has been observed. The linearity of K-L plots shows the first order reaction kinetics followed by the Co_2FeO_4@rGO composite like CFG-10 sample with increasing concentration of dissolved oxygen into electrolytic solution [58, 59]. It

is obvious from the excellent linearity of K-L plots that Co_2FeO_4@rGO composite like CFG-10 has high probability for constant supply of electrons due to its uniform distribution onto the GC electrode, indicating the typical catalytic performance of the composite material.

Furthermore, the effect of rotation per minutes (RPM) at various rates such as 0, 200, 400, 600, and 800 was investigated on ORR activity at a scan rate of 5 mVs^{-1} as shown in Figure 6. There was a linear relationship built with the current density and various values of RPM due to the short distance of electron transport channel between the electrolyte and electrode interfaces designated to variety of active centers available for ORR reaction [60]. The RPM study has revealed an excellent ORR activity by the Co_2FeO_4@rGO composite like CFG-10 sample. Additionally, the effect of various applied potentials on the RPM for understanding the ORR activity of various nanostructured materials was studied as shown in Fig. 6(e). The ORR activity of different nanostructured materials was found static under the used scan rates of 5, 20, 40, 60, 80, 100 and 120 mVs^{-1} as shown as Fig. (S4). This observation has confirmed significant improvement in the ORR activity of Co_2FeO_4@rGO composite like CFG-10 sample.

A general approach has been built to describe ORR reaction mechanism on the carbon based materials involving several steps. The initial step, the adsorption and electron transport take place to produce superoxide (O_2). In next step, either the reduction or disproportionation of superoxide is expected. Under alkaline conditions, two waves are clearly found in ORR polarization curves connected to oxygen reduction or peroxide species taking place at various active centers on the surface of carbon based material [61, 62]. The ORR reaction mechanism on the modified GC electrode is generally followed by reported work [63].

$$GC + O_2 \leftrightarrow GC - O_{2\,(ads)} \quad \text{(i)}$$

$$GC - O_{2\,(ads)} + e^- \rightarrow GC - O^-_{2\,(ads)} \quad \text{(ii)}$$

$$GC - O_{2(ads)} \rightarrow GC - O^-_{2(ads)} \quad \text{(iii)}$$

$$GC - O^-_{2(ads)} + H_2O \rightarrow GC - O_2H_{(ads)} + OH^- \quad \text{(iv)}$$

$$GC - O_2H_{(ads)} + e^- \rightarrow GC - (O_2H)^-_{ads} \quad \text{(v)}$$

$$GC - (O_2H)_{ads} \rightarrow GC + HO_2^- \quad \text{(vi)}$$

The reactant and product described in reaction (iii) are two different forms of superoxide ion on the surface of carbon material [64-66].

Another aspect of water splitting is the OER reaction and it has been considered a very critical for the cathode reaction of rechargeable metal-air batteries and as anode in the overall splitting process [67]. The OER is found kinetically slow half-cell reaction in water splitting as it involves four electron transfer process, therefore an efficient electrocatalyst has to be developed to overcome this challenge in order to exploit complete renewable energy from water splitting.

The OER LSV curves were measured for various synthesized nanostructured materials such as pristine GO, pure cobalt ferrite oxide, 20%RuO_2/C, Co_2FeO_4@rGO composites like CFG-5 and CFG-10 at a scan rate of 5 mVs^{-1} in 1.0 M KOH aqueous solution. The LSV curves of pristine GO and Co2FeO4 have shown relatively poor OER activity with an onset potential of 1.58V and 1.52 V vs RHE. The Co_2FeO_4@rGO composites like CFG-5 and CFG-10 revealed a dramatic decrease in OER onset potential of 1.49V and 1.47V vs RHE respectively as shown in Fig 7(a). The measured overpotentials of pristine GO, pure Co_2FeO_4, Co_2FeO_4@rGO composites like CFG-5 and CFG-10 at 20 mAcm-2 are 350, 290, 260, and 240 mV and these overpotential values have been extracted from the theoretical thermodynamic potential of 1.23 V for water splitting. For better pictorial presentation, the overpotentials of prepared materials are enclosed in Fig. 7(e), highlighting the superior performance of Co_2FeO_4@rGO composite like CFG-10 sample. The OER performance of Co_2FeO_4@rGO composite like CFG-10 in terms of low overpotential was compared with recently published results on nonprecious electrocatalysts supplementary Table (S2). The composite has superior or comparable performance to those excellent developed electrocatalysts. The enhanced performance of Co_2FeO_4@rGO composites could be attributed to several factors such as synergetic effect between cobalt ferrite oxide and GO through active sites from Co_2FeO_4 and electrical conductivity from GO, defects in the structure including oxygen vacancies, morphology of composite materials, large ECSA value, fast charge transport value and an excellent interfacial chemistry between the well chemically anchored cobalt ferrite oxide onto GO [68, 69]. The Tafel analysis was used to study the OER kinetics using Tafel equation as shown in Fig. 7(b). The calculated Tafel slopes are 105, 68, 56 and 51 mVdec-1 for the pristine GO, pure Co_2FeO_4, Co_2FeO_4@rGO composites like CFG-5 and CFG-10 respectively. The Tafel study has

revealed an outstanding OER kinetics on the Co_2FeO_4@rGO composites from practical point of view compare to the noble metal RuO2 based catalysts.

The OER reaction processes via four electron transfer mechanism, generally on the surface of metal oxides under alkaline conditions is described as follows:

$$M + OH^- \rightarrow MOH + e^- \quad (1)$$

$$MOH + OH^- \rightarrow MO^- H_2O \quad (2)$$

$$MO^- \rightarrow MO + e^- \quad (3)$$

$$2MO \rightarrow 2M + O_2 + 2e^- \quad (4)$$

Theoretically, Tafel values are assumed on the basis of above four steps as 120, 60, 40, and 15 $mVdec^{-1}$. In our case, the rate limiting step of OER kinetics is governed by step 2.

The durability and stability are very essential to investigate for the nonprecious electrocatalysts as generally they are limited by these issues for long term applications. This is the reason, we studied the durability of Co_2FeO_4@rGO composite like CFG-10 using chronopotentiometry test at various current densities of 20, 40, 60 mA/cm^2 for 48 hours as shown in Fig. 7(c). These results have shown an excellent durable response of this composite system confirming its potential long term applications. These outstanding durability performance is possibly related to strong chemical coupling of cobalt ferrite oxide onto GO leading to provision of multichannel for charge transport without any abrupt changes. The stability was studied by the comparative analysis of LSV curves before and after the durability experiment as shown in Fig. 7(d), resulting no shift in the osnet potential, current density and overpotential. Therefore, outperform stability is an excellent indicator for Co_2FeO_4@rGO composite like CFG-10 towards long term and large scale applications. To understand the scientific reason during OER process, EIS study was used to quantify the charge transfer resistance value of various nanostructured materials at OER onset potential and 1.0 M KOH solution. The EIS data was analyzed by two ways including Bode plots and Nyquist plots. The Bode plots are enclosed in in supplementary data Fig. (S6) and corresponding Nyquist plots are depicted in Fig. 7(f). The corresponding values from EIS calculation are given in Table 1. The Co2FeO4@GO composite like CFG-10 has shown superior phase angle as compare to CFG-5 and both pristine GO and cobalt ferrite oxide materials. The

charge transfer resistance (R_{ct}) values were 1020, 780.8, 395 and 58.5 Ω for GO, pristine Co_2FeO_4, Co_2FeO_4@rGO composites like CFG-5 and CFG-10 respectively. The low charge transfer resistance of Co_2FeO_4@rGO composite like CFG-10 is again verifying an excellent charge transfer between modified electrode and electrolyte. Hence, accelerated OER kinetics has been demonstrated on the surface of Co_2FeO_4@rGO composite like CFG-10 sample.

In addition to the excellent bi-functional ORR and OER activities, Co_2FeO_4@rGO composite like CFG-10 also demonstrate a significant activity as cathode material towards HER in water splitting. The LSV polarization curves were measured for GO, pristine Co_2FeO_4, Co_2FeO_4@rGO composites like CFG-5 and CFG-10 in 1.0 M KOH at scan rate of 5 mVs^{-1} as shown in Fig. 8(a). The HER performance of these nonprecious nanostructured materials was evaluated with respect to noble metal 20%Pt/C. The measured overpotential of GO, pristine Co_2FeO_4, Co_2FeO_4@rGO composites like CFG-5 and CFG-10 are 470, 420, 380, and 320 at 10 $mAcm^{-2}$. These high values of overpotential suggest that pristine GO and cobalt ferrite oxide have poor HER activity due to few catalytic active centers, consequently limited electrochemical performance is observed. However, the Co_2FeO_4@rGO composites like CFG-5 and CFG-10 have relatively low overpotential and indicating the role of composite material in terms of synergetic effect toward enhanced HER performance. The Co_2FeO_4@rGO composite like CFG-10 has shown superior or comparable performance to those recently reported HER nonprecious electrocatalysts in alkaline conditions as given in Table (S1). This superior performance owned by Co_2FeO_4@rGO composite like CFG-10 is attributed to high density active sites, electrical conductivity, swift electron transfer and favorable surface properties [70, 71]. For better readability and visibility, the measured overpotential of various presented materials are shown in Figure 8(e). The HER kinetics was evaluated in terms of Tafel analysis using Tafel equation and the obtained results are enclosed in Fig. 8(b). The Tafel slopes of GO, pristine Co_2FeO_4, Co_2FeO_4@rGO composites like CFG-5 and CFG-10 were measured as 152, 80, 59 and 48 $mVdec^{-1}$ respectively. The Co_2FeO_4@rGO compsites like CFG-10 has exhibited low Tafel slope value signifying the faster HER kinetics via swift two electron transfer and closely related to that of 20%Pt/C. The chronopotentiometry was used to investigate the durability of Co_2FeO_4@rGO composites like CFG-10 during HER process at different current densities of 10, 20 and 30 $mAcm^{-2}$. The durability results for 48 hours confirmed the outperform performance for lone term applications as depicted in Fig. 8(c). There was no flocculation in potential drop during durability measurement due to strong chemical

bonding between GO and cobalt ferrite oxide resulting to static and fast charge transport during HER reaction. Furthermore, the stability was analyzed through LSV curves behavior before and after the durability measurement as shown in Figure 8(d). The stability results were found satisfactory without any abrupt variation in the onset potential and current density during HER reaction. It has been shown that charge transport during electrochemical HER reaction is essential to determine as it is directly linked to the kinetics of reaction kinetics. Therefore, we have carried out EIS in 1M KOH and the obtained Nyquist plots for the description of charge transfer are shown in Fig. 8(f). However, the Bode plots are enclosed in supplementary Fig. (S6). The charge transfer values of GO, pristine Co_2FeO_4, Co_2FeO_4@rGO composites like CFG-5 and CFG-10 were observed as with corresponding R_{ct} values of 1230, 960.5, 380.75 and 64.8 Ω respectively. The Co_2FeO_4, Co_2FeO_4@rGO composite like CFG-10 exhibited a fast charge transport properties owing to the presence of highly conductive host substrate GO for cobalt ferrite oxide nanostructures, thus revealing a favorable HER kinetics. Under alkaline conditions, the HER kinetics expressed by three step as described in equations (1), (2), and (3) as given below:

$$H_2O + e^- + M \rightarrow MH_{ads} + OH^- \qquad \text{(Volmer step)}$$

$$MH_{ads} + MH_{ads} \rightarrow H_2 + 2M \qquad \text{(Tafel step)}$$

$$H_2O + MH_{ads} + e^- \rightarrow H_2 + M + OH^- \qquad \text{(Heyrovsky step)}$$

The first step is related to Volmer step, which involves the adsorption of protons onto the electrode surface as indicated in equation (1), then followed by the recombination of adsorbed intermediates as represented in equation (2) or Heyrovsky step, which involves the sorption of the adsorbed species as expressed in equation (3) [72]. The HER mechanism on Co_2FeO_4@rGO composite like CFG-10 is followed by Heyrovsky step.

The evaluated high performance electrocatalytic properties of Co_2FeO_4@rGO composite like CFG-10 could be attributed from the following factors. 1. The simultaneous hydrothermal and reduction of has offered high electrical conductive material rGO with unique structure for hosting the cobalt ferrite oxide nanostructures and multi electron transfer channels [73-75]. 2. The use of Fe substituent for the Co enabled the superfast durability of composite material, it eliminates the aggregation of Co during electrochemical reactions, with exposure of optimum catalytic sites, and electrochemical stability [76]. 3. The strong chemical coupling of binary metal oxide with rGO

further excited the composite material to behave efficiently towards ORR, OER and HER leading to its multifunctional applications [77, 78, 79]. The variation in the metal oxidation states and oxygen vacancies at the surface of Co_2FeO_4@rGO composites due to varying amount of GO is responsible for the multifunctional surface properties. 5. The use of in situ cobalt ferrite and rGO process favored the three demanding functionalities of water splitting at the surface of composite system. Moreover, based on the physical characterizations, the improved electrocatalytic multifunctional applications are attributed to defects in the crystal structure of composite as indicated by XRD, small particle size surface and large quantity of rGO of composite provided the favorable surface for frequent interaction of water molecules during electrolysis as revealed from SEM and EDS analysis, HRTEM confirmed the favorable catalytic edges, strong coupling between rGO and cobalt ferrite oxide enable the composite to allow the steady and continuous charge transport without the compromise on the catalytic performance during water splitting, and the presence of variant metallic oxidation states. Additionally, the excellent electrocatalytic activities of Co_2FeO_4@rGO composite like CFG-10 are compared with recently reported multifunctional electrocatalysts (Table S4) confirming as developed Co_2FeO_4@rGO composite like CFG-10 would be an excellent choice in terms of low overpotential, high current density and low cost as an alternative multifunctional electrocatalyst employed in the practical applications of water splitting.

To get deeper insight on the improved multifunctional applications of GO, pristine Co_2FeO_4, Co_2FeO_4@rGO composites like CFG-5 and CFG-10, electrochemically active surface area (ECSA) and double layer capacitance were calculated from the non-faradic region of CV curves at various sweeping scans. The CV curves were recorded against different scan rates such as 30, 50, 70, 90, 110, 130 mVs^{-1} as shown in supplementary Fig. (S5). The C_{dl} values were calculated from CV curves through linear fitting of current density versus different scan rates as depicted in Fig. S5(e). The C_{dl} values have been calculated as 3.1, 7.3, 16.6 and 23.2 $\mu F/cm^2$ for GO, pristine Co_2FeO_4, Co_2FeO_4@rGO composites like CFG-5 and CFG-10 respectively. The ECSA has been calculated through C_{dl} values through following relation;

$$\mathrm{ECSA} = {}^{C_{dl}}/_{C_s}$$

In the given expression, C_{dl} is double layer capacitance and Cs is specific capacitance at the interface of electrode (Cs=0.04 μF/cm^2) for KOH medium. The calculated ECSA values are 77.5, 182.5, 415 and 580 cm^2 for GO, pristine Co_2FeO_4, Co_2FeO_4@rGO composites like CFG-5 and CFG-10 respectively as shown in Table 1. The obtained values of ECSA suggest that, addition of GO at optimum level has dramatically enhanced the active sites of Co_2FeO_4 and they have shown vital role in overall electrochemical performance towards core OER, HER and ORR reactions. The change in the morphology and lattice fringes after the durability test of OER and HER were evaluated by SEM, EDS and HRTEM as shown in S7 and S8. This analysis is suggesting a negligible change in the shape and crystal deformation revealing an outstanding stability of composite material for long term applications.

4. Conclusions

In this study, we have used simultaneous hydrothermal and reduction approach for the synthesis of various composite materials based on cobalt ferrite oxide and reduced graphene oxide. The direct use of GO was intentionally changed into rGO during the preparation of cobalt ferrite oxide nanostructures based hybrid system. The synthesis strategy avoids the use of one step of GO into rGO conversion and provides two step synthesis for the hybrid material based on cobalt ferrite oxide@rGO. The Co_2FeO_4@rGO composite like CFG-10 has demonstrated excellent multifunctional applications towards ORR, OER and HER, the core reactions in water splitting. The composite material has shown remarkable comparable or superior to that noble metal catalysts like Pt/C and RuO2/C owing to its high surface area with exposure of optimum catalytic sites, high electrical conductivity and multiple charge transport channels. The Co_2FeO_4@rGO composite like CFG-10 has exhibited onset potential of 0.60 for ORR, and an overpotential of 240 mV and 320 mV for OER and HER respectively in alkaline media. The chronopotentiometry test at various current densities revealed an outstanding durability for the period of 48 hours suggesting the long term applications of proposed multifunctional electrocatalyst based on Co_2FeO_4@rGO composite like CFG-10. The superior performance of composite is attributed to high active surface area of 580 cm^{2,} defects in the structure, oxygen vacancies, fast charge transport and large exposure of active sites of cobalt ferrite oxide on the surface of reduced graphene oxide. Potentially and

promisingly the advance strategy for the design of multifunctional nonprecious electrocatalysts would be an alternative roadmap to harvest hydrogen fuels from electrochemical water splitting.

Acknowledgments

We would like to thank the platform of National Natural Science Foundation of China (NSFC 51402065 and 51603053), "Spectroscopies et Microscopies des Interfaces" (Laboratory of Physical Chemistry and Microbiology for Materials and the Environment, LCPME, Nancy, France) and A. Renard, Dr. M. Mallet (LCPME) for XPS analysis. We thank you to Professor Alberto Vomiero from Division of Materials Science, Department of Engineering & Mathematics, Luleå University of Technology, 97187 Luleå, Sweden, for valuable pre-review feedback on our paper. We also extend our sincere appreciation to the Researchers Supporting Project number (RSP-2022/79) at King Saud University, Riyadh, Saudi Arabia.

Data Availability Statement

Data available in article supplementary material

5. References

[1] Liang, C., P. Zou, A. Nairan, Y. Zhang, J. Liu, K. Liu, S. Hu, F. Kang, H.J. Fan, and C. Yang, Exceptional performance of hierarchical Ni–Fe oxyhydroxide@NiFe alloy nanowire array electrocatalysts for large current density water splitting. Energy & Environmental Science. 13(2020). 86-95.

[2] Gorlin, Y. and T.F. Jaramillo, A Bifunctional Nonprecious Metal Catalyst for Oxygen Reduction and Water Oxidation. Journal of the American Chemical Society. 132(2010). 13612-13614.

[3] Sultan, S., M.H. Diorizky, M. Ha, J.N. Tiwari, H. Choi, N.K. Dang, P. Thangavel, J.H. Lee, H.Y. Jeong, H.S. Shin, Y. Kwon, and K.S. Kim, Modulation of Cu and Rh single-atoms and nanoparticles for high-performance hydrogen evolution activity in acidic media. Journal of Materials Chemistry A. 9(2021). 10326-10334.

[4] Zhang, Y., S. Kumar, F. Marken, M. Krasny, E. Roake, S. Eslava, S. Dunn, E. Da Como, and C.R. Bowen, Pyro-electrolytic water splitting for hydrogen generation. Nano Energy. 58(2019). 183-191.

[5] Guan, C., W. Zhao, Y. Hu, Z. Lai, X. Li, S. Sun, H. Zhang, A.K. Cheetham, and J. Wang, Cobalt oxide and N-doped carbon nanosheets derived from a single two-dimensional metal–organic framework precursor and their application in flexible asymmetric supercapacitors. Nanoscale Horizons. 2(2017). 99-105.

[6] Chen, Z., X. Duan, W. Wei, S. Wang and B.-J. Ni, Iridium-based nanomaterials for electrochemical water splitting. Nano Energy. 78(2020). 105270.

[7] Ren, X., H. Fan, C. Wang, J. Ma, H. Li, M. Zhang, S. Lei, and W. Wang, Wind energy harvester based on coaxial rotatory freestanding triboelectric nanogenerators for self-powered water splitting. Nano Energy. 50(2018). 562-570.

[8] Ramakrishnan, S., J. Balamurugan, M. Vinothkannan, A.R. Kim, S. Sengodan, and D.J. Yoo, Nitrogen-doped graphene encapsulated FeCoMoS nanoparticles as advanced trifunctional catalyst for water splitting devices and zinc–air batteries. Applied Catalysis B: Environmental. 279(2020). 119381.

[9] Zhang, M., Q. Dai, H. Zheng, M. Chen and L. Dai, Novel MOF-Derived Co@N-C Bifunctional Catalysts for Highly Efficient Zn-Air Batteries and Water Splitting. Advanced materials. 30 10(2018).

[10] Li, Y. and H. Dai, Recent advances in zinc–air batteries. Chemical Society Reviews. 43(2014). 5257-5275.

[11] Zhang, Q., B. He, L. Tang, Z. Zhou, L. Kang, J. Sun, T. Zhang, Q. Li, C. Li, J. Zhao, Z. Zhang, L. Wei, and Y. Yao, Fully Solar-Powered Uninterrupted Overall Water-Splitting Systems. Advanced Functional Materials. 29(2019). 1808889.

[12] Yin, J., Y. Li, F. Lv, M. Lu, K. Sun, W. Wang, L. Wang, F. Cheng, Y. Li, P. Xi, and S. Guo, Oxygen Vacancies Dominated NiS2 /CoS2 Interface Porous Nanowires for Portable Zn-Air Batteries Driven Water Splitting Devices. Advanced materials. 29 47(2017).

[13] Sun, H., Q. Li, Y. Lian, C. Zhang, P. Qi, Q. Mu, H. Jin, B. Zhang, M. Chen, Z. Deng, and Y. Peng, Highly efficient water splitting driven by zinc-air batteries with a single catalyst incorporating rich active species. Applied Catalysis B: Environmental. 263(2020). 118139.

[14] Zhang, J., Z. Zhao, Z. Xia and L. Dai, A metal-free bifunctional electrocatalyst for oxygen reduction and oxygen evolution reactions. Nature Nanotechnology. 10(2015). 444-452.
[15] Hunter, B.M., H.B. Gray and A.M. Müller, Earth-Abundant Heterogeneous Water Oxidation Catalysts. Chemical Reviews. 116(2016). 14120-14136.
[16] Pei, Z., Z. Tang, Z. Liu, Y. Huang, Y. Wang, H. Li, Q. Xue, M. Zhu, D. Tang, and C. Zhi, Construction of a hierarchical 3D Co/N-carbon electrocatalyst for efficient oxygen reduction and overall water splitting. Journal of Materials Chemistry A. 6(2018). 489-497.
[17] Tang, B., J. Yang, Z. Kou, L. Xu, H.L. Seng, Y. Xie, A.D. Handoko, X. Liu, Z.W. Seh, H. Kawai, H. Gong, and W. Yang, Surface-engineered cobalt oxide nanowires as multifunctional electrocatalysts for efficient Zn-Air batteries-driven overall water splitting. Energy Storage Materials. 23(2019). 1-7.
[18] Ma, L., S. Chen, Z. Pei, Y. Huang, G. Liang, F. Mo, Q. Yang, J. Su, Y. Gao, J.A. Zapien, and C. Zhi, Single-Site Active Iron-Based Bifunctional Oxygen Catalyst for a Compressible and Rechargeable Zinc–Air Battery. ACS Nano. 12(2018). 1949-1958.
[19] Guan, C., A. Sumboja, H. Wu, W. Ren, X. Liu, H. Zhang, Z. Liu, C. Cheng, S.J. Pennycook, and J. Wang, Hollow Co(3) O(4) Nanosphere Embedded in Carbon Arrays for Stable and Flexible Solid-State Zinc-Air Batteries. Adv Mater. 29(2017).
[20] Zhu, L., D. Zheng, Z. Wang, X. Zheng, P. Fang, J. Zhu, M. Yu, Y. Tong, and X. Lu, A Confinement Strategy for Stabilizing ZIF-Derived Bifunctional Catalysts as a Benchmark Cathode of Flexible All-Solid-State Zinc-Air Batteries. Adv Mater. 30(2018). e1805268.
[21] Amiinu, I.S., Z. Pu, X. Liu, K.A. Owusu, H.G.R. Monestel, F.O. Boakye, H. Zhang, and S. Mu, Multifunctional Mo-N/C@MoS2Electrocatalysts for HER, OER, ORR, and Zn-Air Batteries. Advanced Functional Materials. 27(2017). 1702300.
[22] Lefèvre, M., E. Proietti, F. Jaouen and J.-P. Dodelet, Iron-Based Catalysts with Improved Oxygen Reduction Activity in Polymer Electrolyte Fuel Cells. Science. 324(2009). 71-74.
[23] Cui, C., L. Gan, M. Heggen, S. Rudi and P. Strasser, Compositional segregation in shaped Pt alloy nanoparticles and their structural behaviour during electrocatalysis. Nat Mater. 12(2013). 765-71.
[24] Wang, M., W. Zhang, J. Wang, A. Minett, V. Lo, H. Liu, and J. Chen, Mesoporous hollow PtCu nanoparticles for electrocatalytic oxygen reduction reaction. Journal of Materials Chemistry A. 1(2013). 2391-2394.
[25] Zhou, L., D. Zhao and X. Lou, LiNi(0.5)Mn(1.5)O4 hollow structures as high-performance cathodes for lithium-ion batteries. Angew Chem Int Ed Engl. 51(2012). 239-41.
[26] Rakhi, R.B., W. Chen, D. Cha and H.N. Alshareef, Substrate Dependent Self-Organization of Mesoporous Cobalt Oxide Nanowires with Remarkable Pseudocapacitance. Nano Letters. 12(2012). 2559-2567.
[27] Liu, Z.Q., H. Cheng, N. Li, T.Y. Ma and Y.Z. Su, ZnCo2 O4 Quantum Dots Anchored on Nitrogen-Doped Carbon Nanotubes as Reversible Oxygen Reduction/Evolution Electrocatalysts. Adv Mater. 28(2016). 3777-84.
[28] Cheng, H., M.-L. Li, C.-Y. Su, N. Li and Z.-Q. Liu, Cu□Co Bimetallic Oxide Quantum Dot Decorated Nitrogen-Doped Carbon Nanotubes: A High-Efficiency Bifunctional

Oxygen Electrode for Zn-Air Batteries. Advanced Functional Materials. 27(2017). 1701833.
[29] Wang, H., R. Liu, Y. Li, X. Lü, Q. Wang, S. Zhao, K. Yuan, Z. Cui, X. Li, S. Xin, R. Zhang, M. Lei, and Z. Lin, Durable and Efficient Hollow Porous Oxide Spinel Microspheres for Oxygen Reduction. Joule. 2(2018). 337-348.
[30] Zhang, L., J.C. Yu, Z. Zheng and C.W. Leung, Fabrication of hierarchical porous iron oxide films utilizing the Kirkendall effect. Chemical Communications, (2005). 2683-2685.
[31] Fan, H.J., U. Gosele and M. Zacharias, Formation of nanotubes and hollow nanoparticles based on Kirkendall and diffusion processes: a review. Small. 3(2007). 1660-71.
[32] Xie, Y. and C. Wu, Design of nanoarchitectured electrode materials applied in new-generation rechargeable lithium ion batteries. Dalton Trans, (2007). 5235-40.
[33] Wang, D., S. Lu and S.P. Jiang, Pd/HPW-PDDA-MWCNTs as effective non-Pt electrocatalysts for oxygen reduction reaction of fuel cells. Chemical Communications. 46(2010). 2058-2060.
[34] Wang, X.T., T. Ouyang, L. Wang, J.H. Zhong, T. Ma, and Z.Q. Liu, Redox-Inert Fe(3+) Ions in Octahedral Sites of Co-Fe Spinel Oxides with Enhanced Oxygen Catalytic Activity for Rechargeable Zinc-Air Batteries. Angew Chem Int Ed Engl. 58(2019). 13291-13296.
[35] Liang, Y., Y. Li, H. Wang, J. Zhou, J. Wang, T. Regier, and H. Dai, Co_3O_4 nanocrystals on graphene as a synergistic catalyst for oxygen reduction reaction. Nat Mater. 10(2011). 780-6.
[36] Wang, J., H.L. Xin, J. Zhu, S. Liu, Z. Wu, and D. Wang, 3D hollow structured Co2FeO4/MWCNT as an efficient non-precious metal electrocatalyst for oxygen reduction reaction. Journal of Materials Chemistry A. 3(2015). 1601-1608.
[37] Narwade, S.S., S.M. Mali, V.S. Sapner and B.R. Sathe, Graphene Oxide Decorated with Rh Nanospheres for Electrocatalytic Water Splitting. ACS Applied Nano Materials. 3(2020). 12288-12296.
[38] Choi, S., C. Kim, J.M. Suh and H.W. Jang, Reduced graphene oxide-based materials for electrochemical energy conversion reactions. Carbon Energy. 1(2019). 85-108.
[39] Dreyer, D.R., S. Park, C.W. Bielawski and R.S. Ruoff, The chemistry of graphene oxide. Chemical Society Reviews. 39(2010). 228-240.
[40] Park, S. and R.S. Ruoff, Chemical methods for the production of graphenes. Nature Nanotechnology. 4(2009). 217-224.
[41] Jeon, J.M., T.L. Kim, Y.S. Shim, Y.R. Choi, S. Choi, S. Lee, K.C. Kwon, S.H. Hong, Y.W. Kim, S.Y. Kim, M. Kim, and H.W. Jang, Microscopic Evidence for Strong Interaction between Pd and Graphene Oxide that Results in Metal-Decoration-Induced Reduction of Graphene Oxide. Adv Mater. 29(2017).
[42] Zaaba, N.I., K.L. Foo, U. Hashim, S.J. Tan, W.-W. Liu, and C.H. Voon, Synthesis of Graphene Oxide using Modified Hummers Method: Solvent Influence. Procedia Engineering. 184(2017). 469-477.
[43] Yu, H., B. Zhang, C. Bulin, R. Li and R. Xing, High-efficient Synthesis of Graphene Oxide Based on Improved Hummers Method. Scientific Reports. 6(2016). 36143.
[44] Muniyalakshmi, M., K. Sethuraman and D. Silambarasan, Synthesis and characterization of graphene oxide nanosheets. Materials Today: Proceedings. 21(2020). 408-410.

[45] Aliyari, E., M. Alvand and F. Shemirani, Modified surface-active ionic liquid-coated magnetic graphene oxide as a new magnetic solid phase extraction sorbent for preconcentration of trace nickel. RSC Advances. 6(2016). 64193-64202.
[46] Ravindra, A.V., M. Chandrika, C. Rajesh, P. Kollu, S. Ju, and S.D. Ramarao, Simple synthesis, structural and optical properties of cobalt ferrite nanoparticles. The European Physical Journal Plus. 134(2019). 296.
[47] Yang, J., Z. Yang, T. Meng, Y. Han, X. Wang, and Q. Zhang, Effects of silicon doping on the performance of tin oxide thin film transistors. physica status solidi (a). 213(2016). 1010-1015.
[48] Xiong, D., X. Wang, W. Li and L. Liu, Facile synthesis of iron phosphide nanorods for efficient and durable electrochemical oxygen evolution. Chem Commun (Camb). 52(2016). 8711-4.
[49] Zhao, Q., L. Fu, D. Jiang, J. Ouyang, Y. Hu, H. Yang, and Y. Xi, Nanoclay-modulated oxygen vacancies of metal oxide. Communications Chemistry. 2(2019).
[50] Lei, F., Y. Sun, K. Liu, S. Gao, L. Liang, B. Pan, and Y. Xie, Oxygen vacancies confined in ultrathin indium oxide porous sheets for promoted visible-light water splitting. J Am Chem Soc. 136(2014). 6826-9.
[51] Sun, M., H. Liu, Y. Liu, J. Qu and J. Li, Graphene-based transition metal oxide nanocomposites for the oxygen reduction reaction. Nanoscale. 7(2015). 1250-1269.
[52] Sharma, N., V. Sharma, R. Vyas, M. Kumari, A. Kaushal, R. Gupta, S.K. Sharma, and K. Sachdev, A new sustainable green protocol for production of reduced graphene oxide and its gas sensing properties. Journal of Science: Advanced Materials and Devices. 4(2019). 473-482.
[53] Sagu, J.S., K.G.U. Wijayantha and A.A. Tahir, The Pseudocapacitive Nature of CoFe2O4 Thin Films. Electrochimica Acta. 246(2017). 870-878.
[54] Kasztelan, M., A. Słoniewska, M. Gorzkowski, A. Lewera, B. Pałys, and S. Zoladek, Ammonia modified graphene oxide – Gold nanoparticles composite as a substrate for surface enhanced Raman spectroscopy. Applied Surface Science. 554(2021). 149060.
[55] Venkatesan, K., D. Rajan Babu, M.P. Kavya Bai, R. Supriya, R. Vidya, S. Madeswaran, P. Anandan, M. Arivanandhan, and Y. Hayakawa, Structural and magnetic properties of cobalt-doped iron oxide nanoparticles prepared by solution combustion method for biomedical applications. International journal of nanomedicine. 10 Suppl 1(2015). 189-198.
[56] Chaki, S.H., T.J. Malek, M.D. Chaudhary, J.P. Tailor and M.P. Deshpande, Magnetite Fe3O4nanoparticles synthesis by wet chemical reduction and their characterization. Advances in Natural Sciences: Nanoscience and Nanotechnology. 6(2015). 035009.
[57] Sharma, J.K., P. Srivastava, G. Singh, M.S. Akhtar and S. Ameen, Green synthesis of Co3O4 nanoparticles and their applications in thermal decomposition of ammonium perchlorate and dye-sensitized solar cells. Materials Science and Engineering: B. 193(2015). 181-188.
[58] Pei, Z., J. Zhao, Y. Huang, Y. Huang, M. Zhu, Z. Wang, Z. Chen, and C. Zhi, Toward enhanced activity of a graphitic carbon nitride-based electrocatalyst in oxygen reduction and hydrogen evolution reactions via atomic sulfur doping. Journal of Materials Chemistry A. 4(2016). 12205-12211.
[59] Pan, Z., H. Chen, J. Yang, Y. Ma, Q. Zhang, Z. Kou, X. Ding, Y. Pang, L. Zhang, Q. Gu, C. Yan, and J. Wang, CuCo2S4 Nanosheets@N-Doped Carbon Nanofibers by

Sulfurization at Room Temperature as Bifunctional Electrocatalysts in Flexible Quasi-Solid-State Zn-Air Batteries. Adv Sci (Weinh). 6(2019). 1900628.
[60] Hu, M., X. Li, J. Xiong, L. Zeng, Y. Huang, Y. Wu, G. Cao, and W. Li, Nano-Fe3C@PGC as a novel low-cost anode electrocatalyst for superior performance microbial fuel cells. Biosensors & bioelectronics. 142(2019). 111594-111594.
[61] Li, X., M. Hu, L. Zeng, J. Xiong, B. Tang, Z. Hu, L. Xing, Q. Huang, and W. Li, Co-modified MoO2 nanoparticles highly dispersed on N-doped carbon nanorods as anode electrocatalyst of microbial fuel cells. Biosensors & bioelectronics. 145(2019). 111727.
[62] Tian, J., W. Wu, Z. Tang, Y. Wu, R. Burns, B. Tichnell, Z. Liu, and S. Chen, Oxygen Reduction Reaction and Hydrogen Evolution Reaction Catalyzed by Pd–Ru Nanoparticles Encapsulated in Porous Carbon Nanosheets. Catalysts. 8(2018). 329.
[63] Zhou, R., Y. Zheng, M. Jaroniec and S.-Z. Qiao, Determination of the Electron Transfer Number for the Oxygen Reduction Reaction: From Theory to Experiment. ACS Catalysis. 6(2016). 4720-4728.
[64] Choi, S., J. Kwon, S. Jo, S. Kim, K. Park, S. Kim, H. Han, U. Paik, and T. Song, Highly efficient and stable bifunctional electrocatalysts with decoupled active sites for hydrogen evolution and oxygen reduction reactions. Applied Catalysis B: Environmental. 298(2021). 120530.
[65] Chakrabarty, S., A. Mukherjee, W.-N. Su and S. Basu, Improved bi-functional ORR and OER catalytic activity of reduced graphene oxide supported ZnCo2O4 microsphere. International Journal of Hydrogen Energy. 44(2019). 1565-1578.
[66] Li, Y., Q. Li, H. Wang, L. Zhang, D.P. Wilkinson, and J. Zhang, Recent Progresses in Oxygen Reduction Reaction Electrocatalysts for Electrochemical Energy Applications. Electrochemical Energy Reviews. 2(2019). 518-538.
[67] Yeager, E., Dioxygen electrocatalysis: mechanisms in relation to catalyst structure. Journal of Molecular Catalysis. 38(1986). 5-25.
[68] Wang, D.-C., N.-B. Huang, Y. Sun, S. Zhan and J.-J. Zhang, GO clad Co3O4 (Co3O4@GO) as ORR catalyst of anion exchange membrane fuel cell. International Journal of Hydrogen Energy. 42(2017). 20216-20223.
[69] Li, H., Y. Huang, H. Zhou, W. Yang, M. Li, Z. Huang, C. Fu, and Y. Kuang, One step in-situ synthesis of Co@N, S co-doped CNTs composite with excellent HER and ORR bi-functional electrocatalytic performances. Electrochimica Acta. 247(2017). 736-744.
[70] Quílez-Bermejo, J., E. Morallón and D. Cazorla-Amorós, Metal-free heteroatom-doped carbon-based catalysts for ORR: A critical assessment about the role of heteroatoms. Carbon. 165(2020). 434-454.
[71] Yan, Y., Y. Xu, B. Zhao, Y. Xu, Y. Gao, G. Chen, W. Wang, and B.Y. Xia, Bifunctional nickel ferrite-decorated carbon nanotube arrays as free-standing air electrode for rechargeable Zn–air batteries. Journal of Materials Chemistry A. 8(2020). 5070-5077.
[72] Zhao, Y., S. Chen, B. Sun, D. Su, X. Huang, H. Liu, Y. Yan, K. Sun, and G. Wang, Graphene-Co3O4 nanocomposite as electrocatalyst with high performance for oxygen evolution reaction. Scientific Reports. 5(2015). 7629.
[73] Li, M., C. Bao, Y. Liu, J. Meng, X. Liu, Y. Cai, D. Wuu, Y. Zong, T.-P. Loh, and Z. Wang, Reduced graphene oxide-supported cobalt oxide decorated N-doped graphitic carbon for efficient bifunctional oxygen electrocatalysis. RSC Advances. 9(2019). 16534-16540.

[74] Tang, Y., K. Lan, F. Li, P.B. Jiang, X. Wang, Y.Y. Yang, W.B. Gao, B. Wang, and R. Li, Reduced graphene oxide-supported Ni-MoxC electrocatalyst for hydrogen evolution reaction prepared by ultrasonication and lyophilization. International Journal of Hydrogen Energy. 44(2019). 9328-9337.
[75] Makhafola, M.D., K.D. Modibane, K.E. Ramohlola, T.C. Maponya, M.J. Hato, K. Makgopa, and E.I. Iwuoha, Palladinized graphene oxide-MOF induced coupling of Volmer and Heyrovsky mechanisms, for the amplification of the electrocatalytic efficiency of hydrogen evolution reaction. Scientific Reports. 11(2021). 17219.
[76] QayoomMugheri, A., AneelaTahira, U. Aftab, M. IshaqAbro, S.R. Chaudhry, L. Amaral, and Z.H. Ibupoto, Co3O4/ NiO bifunctional electrocatalyst for water splitting. Electrochimica Acta. 306(2019). 9-17.
[77] Guan, C., A. Sumboja, W. Zang, Y. Qian, H. Zhang, X. Liu, Z. Liu, D. Zhao, S.J. Pennycook, and J. Wang, Decorating Co/CoNx nanoparticles in nitrogen-doped carbon nanoarrays for flexible and rechargeable zinc-air batteries. Energy Storage Materials. 16(2019). 243-250.
[78] Qiu, W., Y. Li, A. You, Z. Zhang, G. Li, X. Lu, and Y. Tong, High-performance flexible quasi-solid-state Zn–MnO2 battery based on MnO2 nanorod arrays coated 3D porous nitrogen-doped carbon cloth. Journal of Materials Chemistry A. 5(2017). 14838-14846.
[79] Zhong, Y., Z. Pan, X. Wang, J. Yang, Y. Qiu, S. Xu, Y. Lu, Q. Huang, and W. Li, Hierarchical Co(3)O(4) Nano-Micro Arrays Featuring Superior Activity as Cathode in a Flexible and Rechargeable Zinc-Air Battery. Adv Sci (Weinh). 6(2019). 1802243.

Figure Captions

Fig. 1 X-ray diffraction patterns of GO, Co_2FeO_4, CFG-5 composite and CFG-10 composite

Fig. 2 SEM images of various nanostructures with relevant EDS spectra (a) GO (b) Co_2FeO_4 (c) CFG-5 composite and (d) CFG-10 composite

Fig. 3 HRTEM images of various nanostructures and lattice fringes with corresponding FFT pattern (a) Co_2FeO_4 (b) GO (c) CFG-5 composite (d) CFG-10 composite

Fig. 4 XPS spectra for the O1s signal of (a) CFG-5 composite and (b) CFG-10 composite, for the Fe2p signal of (c) CFG-5 composite and (d) CFG-10 composite and the Co2p signal of (e) CFG-5 composite and (f) CFG-10 composite

Fig. 5 (a) LSV curves for ORR activity in 1M KOH solution at 800 RPM with reference of Pt/C (b) Calculated half wave potential values for each nanostructure (c) The Koutecky-Levich (K-L) plots for CFG-10 composite at various potentials

Fig. 6 LSV curves for ORR performance of various nanostructures at 5 mV/s for different RPMs and potentials respectively (a) GO (b) Co_2FeO_4 (c) CFG-5 composite (d) CFG-10 composite and (e) Corresponding linear fitting of current density vs RPM for ORR activity of each nanostructure at fixed 0.4 V potential

Fig. 7 (a) LSV curves of various nanostructures like Co_2FeO_4, GO, Co_2FeO_4@rGO composites (CFG-5 and CFG-10), 20%RuO_2/C at 5 mV/s for OER performance (b) Corresponding Tafel plots (c) Chronopotentiometry durability of Co_2FeO_4@rGO composite (CFG-10), at different current density values of 20, 40 and 60 mA/cm^2 (d) Stability before and after durability test of Co_2FeO_4@rGO composite (CFG-10), (e) Histogram for overpotential values of Co_2FeO_4, GO, Co_2FeO_4@rGO composites (CFG-5 and CFG-10), (f) Nyquist plots for OER performance through EIS study of Co_2FeO_4, GO, Co_2FeO_4@rGO composites (CFG-5 and CFG-10)

Fig. 8 (a) LSV curves of various materials like Co_2FeO_4, GO, Co_2FeO_4@rGO composites (CFG-5 and CFG-10), 20%Pt/C at 5 mV/s for HER performance (b) Corresponding Tafel plots (c) Chronopotentiometry durability of Co_2FeO_4@rGO composites (CFG-10), at 10, 20 and 30 mA/cm^2 (d) stability before and after durability of Co_2FeO_4@rGO composite (CFG-10), (e) Histogram for overpotential values of Co_2FeO_4, GO, Co_2FeO_4@rGO composites (CFG-5 and CFG-10), (f) Nyquist plots for HER performance through EIS study of Co_2FeO_4, GO, Co_2FeO_4@rGO composites (CFG-5 and CFG-10)

Fig. 1

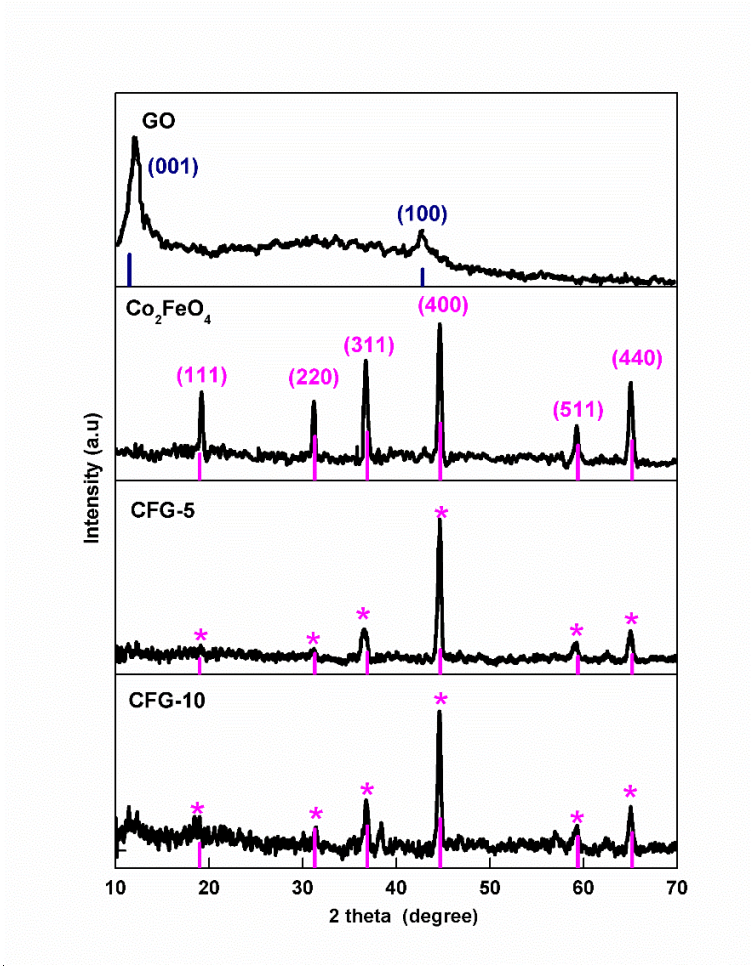
GO
(001)
(100)
Co2FeO4
(400)
(311)
(111)
(220)
(440)
(511)
CFG-5
CFG-10
Intensity (a.u)
10
20
30
40
50
60
70
2 theta (degree)

Fig. 2

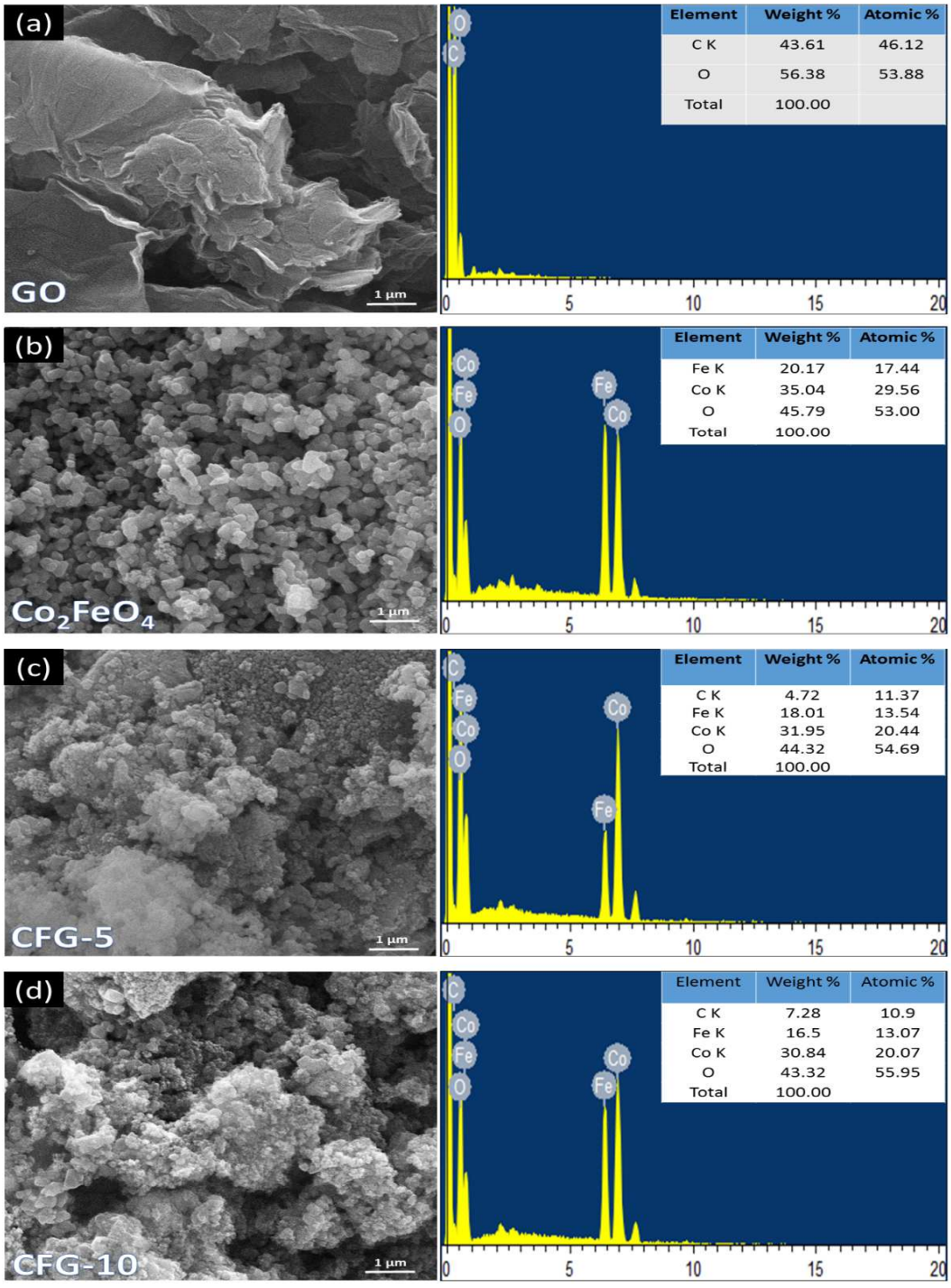
(a)
GO
1 µm
O
C
Element | Weight % | Atomic %
C K | 43.61 | 46.12
O | 56.38 | 53.88
Total | 100.00
0 5 10 15 20
(b)
Co2FeO4
1 µm
Co
Fe
O
Element | Weight % | Atomic %
Fe K | 20.17 | 17.44
Co K | 35.04 | 29.56
O | 45.79 | 53.00
Total | 100.00
0 5 10 15 20
(c)
CFG-5
1 µm
C
Fe
Co
O
Element | Weight % | Atomic %
C K | 4.72 | 11.37
Fe K | 18.01 | 13.54
Co K | 31.95 | 20.44
O | 44.32 | 54.69
Total | 100.00
0 5 10 15 20
(d)
CFG-10
1 µm
C
Co
Fe
O
Element | Weight % | Atomic %
C K | 7.28 | 10.9
Fe K | 16.5 | 13.07
Co K | 30.84 | 20.07
O | 43.32 | 55.95
Total | 100.00
0 5 10 15 20

Fig. 3

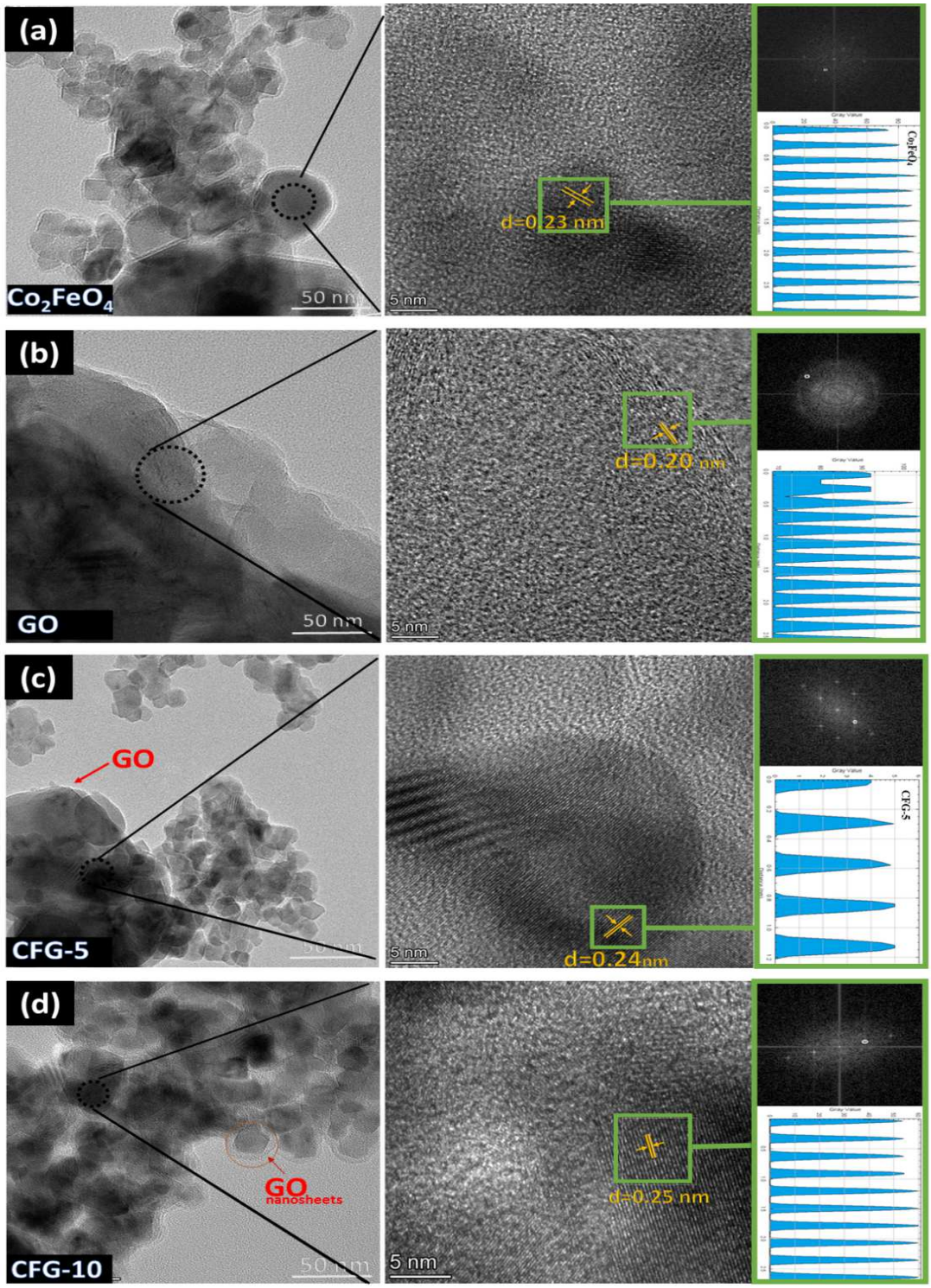
(a)
Co_2FeO_4
50 nm
5 nm
d=0.23 nm
(b)
GO
50 nm
5 nm
d=0.20 nm
(c)
GO
CFG-5
5 nm
d=0.24nm
(d)
GO
nanosheets
CFG-10
5 nm
d=0.25 nm

Fig. 4

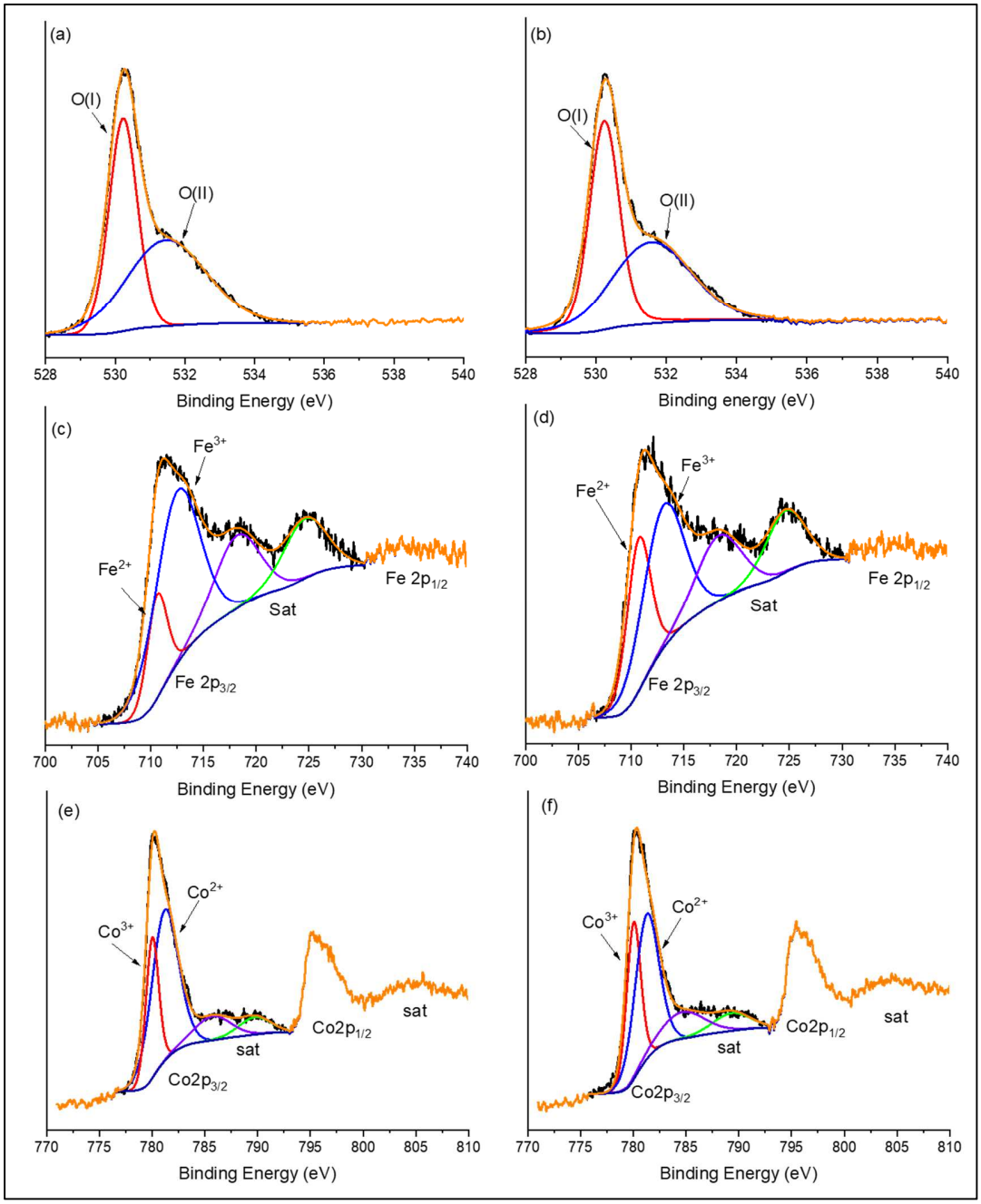
(a)
O(I)
O(II)
528 530 532 534 536 538 540
Binding Energy (eV)
(b)
O(I)
O(II)
528 530 532 534 536 538 540
Binding energy (eV)
(c)
Fe3+
Fe2+
Fe 2p1/2
Sat
Fe 2p3/2
700 705 710 715 720 725 730 735 740
Binding Energy (eV)
(d)
Fe2+
Fe3+
Fe 2p1/2
Sat
Fe 2p3/2
700 705 710 715 720 725 730 735 740
Binding Energy (eV)
(e)
Co2+
Co3+
sat
Co2p1/2
sat
Co2p3/2
770 775 780 785 790 795 800 805 810
Binding Energy (eV)
(f)
Co2+
Co3+
sat
Co2p1/2
sat
Co2p3/2
770 775 780 785 790 795 800 805 810
Binding Energy (eV)

Fig. 5

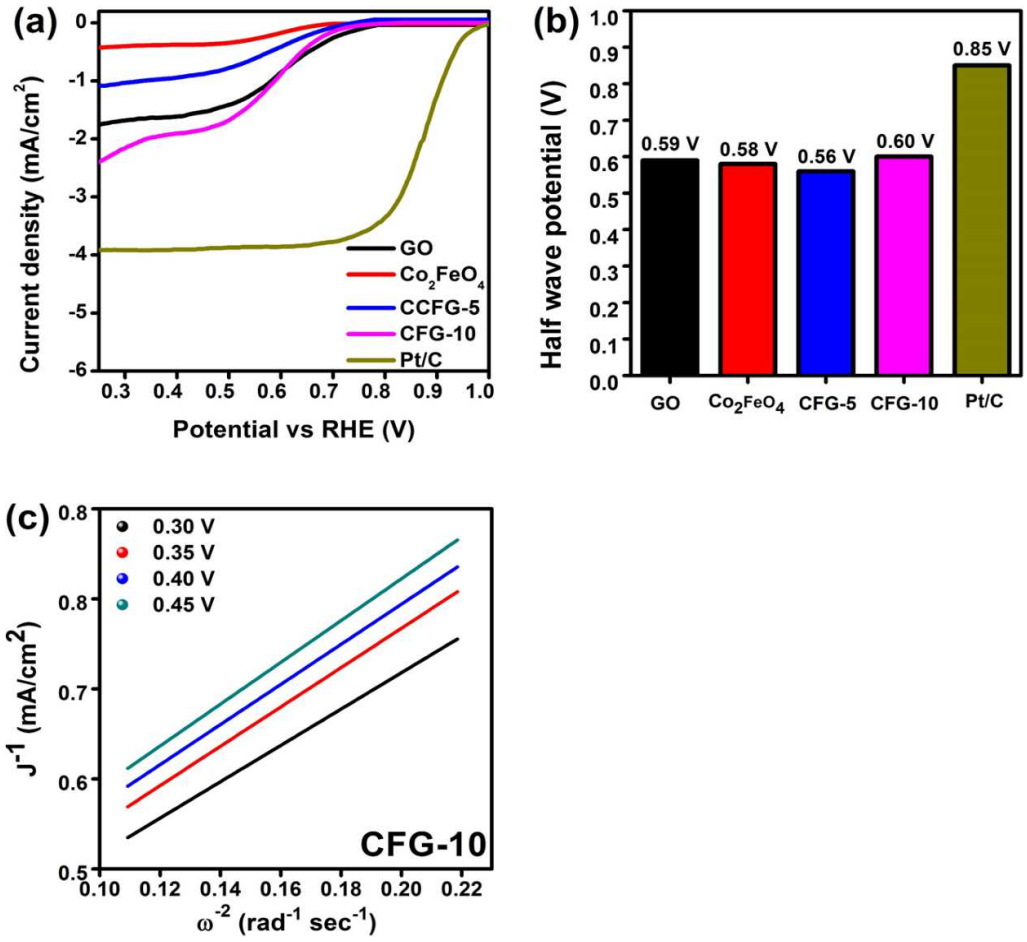
(a)
Current density (mA/cm^2)
Potential vs RHE (V)
GO
Co_2FeO_4
CCFG-5
CFG-10
Pt/C
(b)
Half wave potential (V)
0.59 V
0.58 V
0.56 V
0.60 V
0.85 V
GO
Co_2FeO_4
CFG-5
CFG-10
Pt/C
(c)
0.30 V
0.35 V
0.40 V
0.45 V
CFG-10
J^{-1} (mA/cm^2)
ω^{-2} (rad^{-1} sec^{-1})

Fig. 6

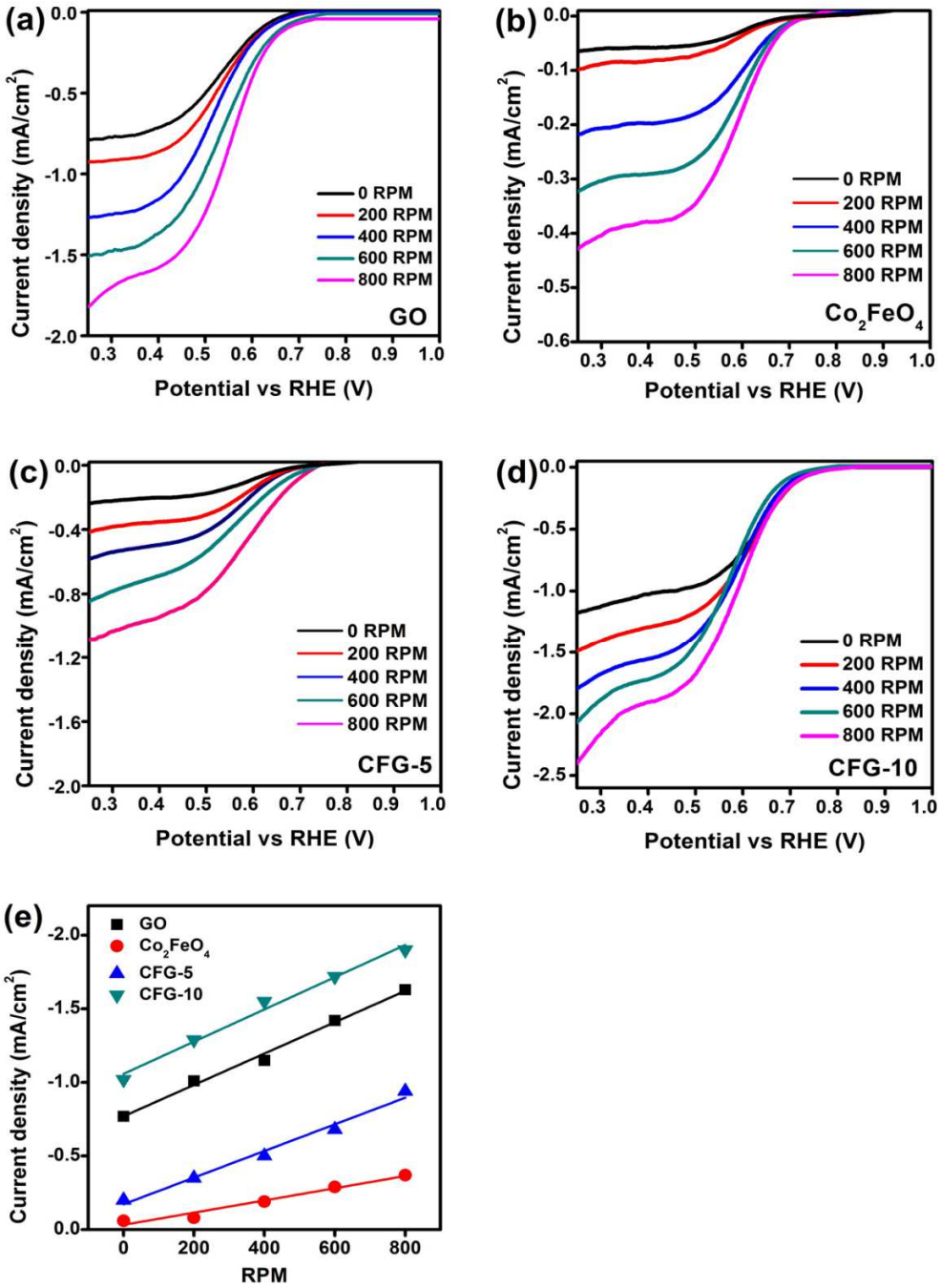
(a)
Current density (mA/cm^2)
Potential vs RHE (V)
0 RPM
200 RPM
400 RPM
600 RPM
800 RPM
GO
(b)
Co_2FeO_4
(c)
CFG-5
(d)
CFG-10
(e)
GO
Co_2FeO_4
CFG-5
CFG-10
RPM

Fig. 7

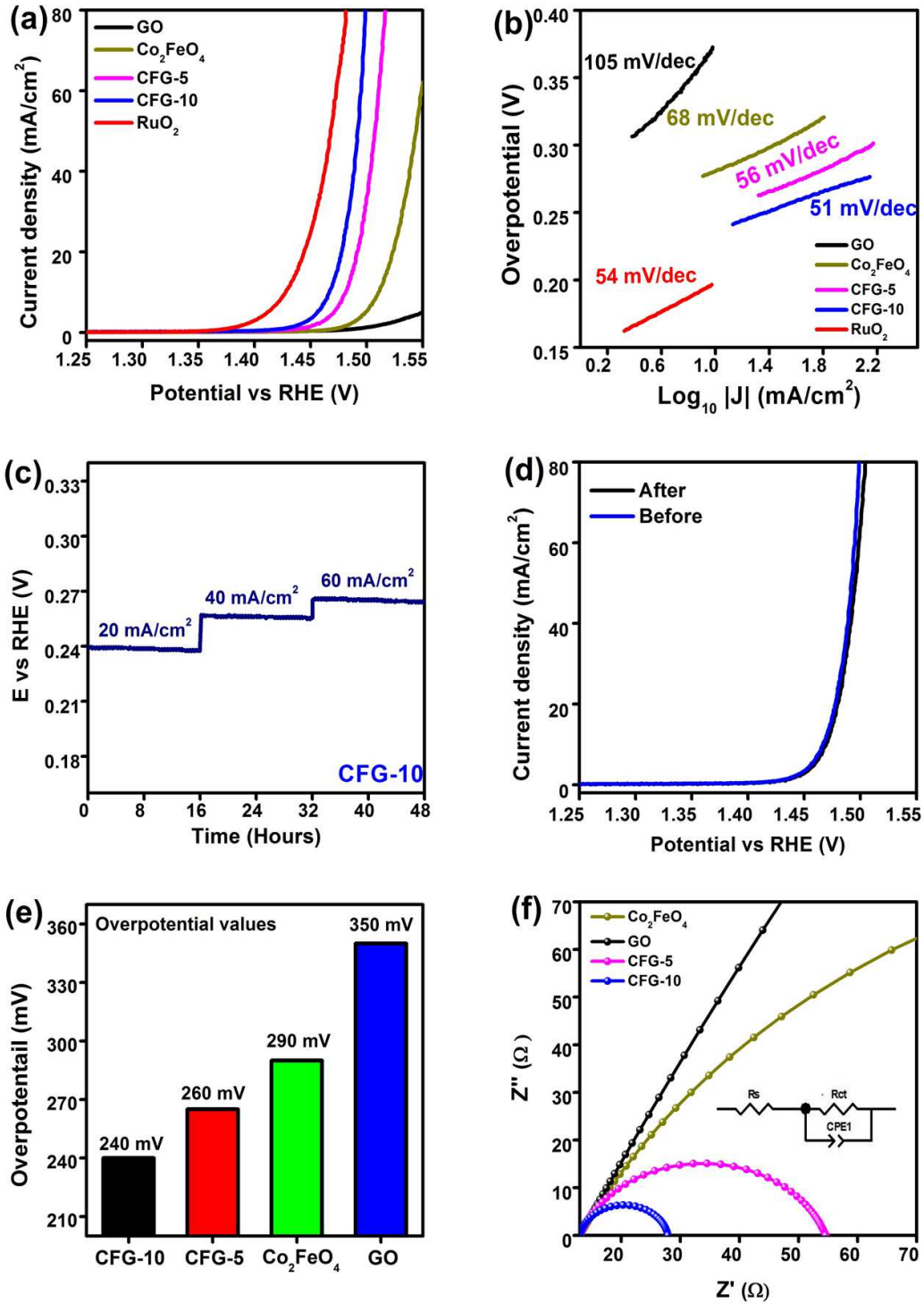
(a)
GO
Co2FeO4
CFG-5
CFG-10
RuO2
Current density (mA/cm2)
Potential vs RHE (V)
(b)
105 mV/dec
68 mV/dec
56 mV/dec
51 mV/dec
54 mV/dec
Overpotential (V)
Log10 |J| (mA/cm2)
(c)
20 mA/cm2
40 mA/cm2
60 mA/cm2
CFG-10
E vs RHE (V)
Time (Hours)
(d)
After
Before
Current density (mA/cm2)
Potential vs RHE (V)
(e)
Overpotential values
240 mV
260 mV
290 mV
350 mV
Overpotentail (mV)
CFG-10
CFG-5
Co2FeO4
GO
(f)
Co2FeO4
GO
CFG-5
CFG-10
Rs
Rct
CPE1
Z'' (Ω)
Z' (Ω)

Fig. 8

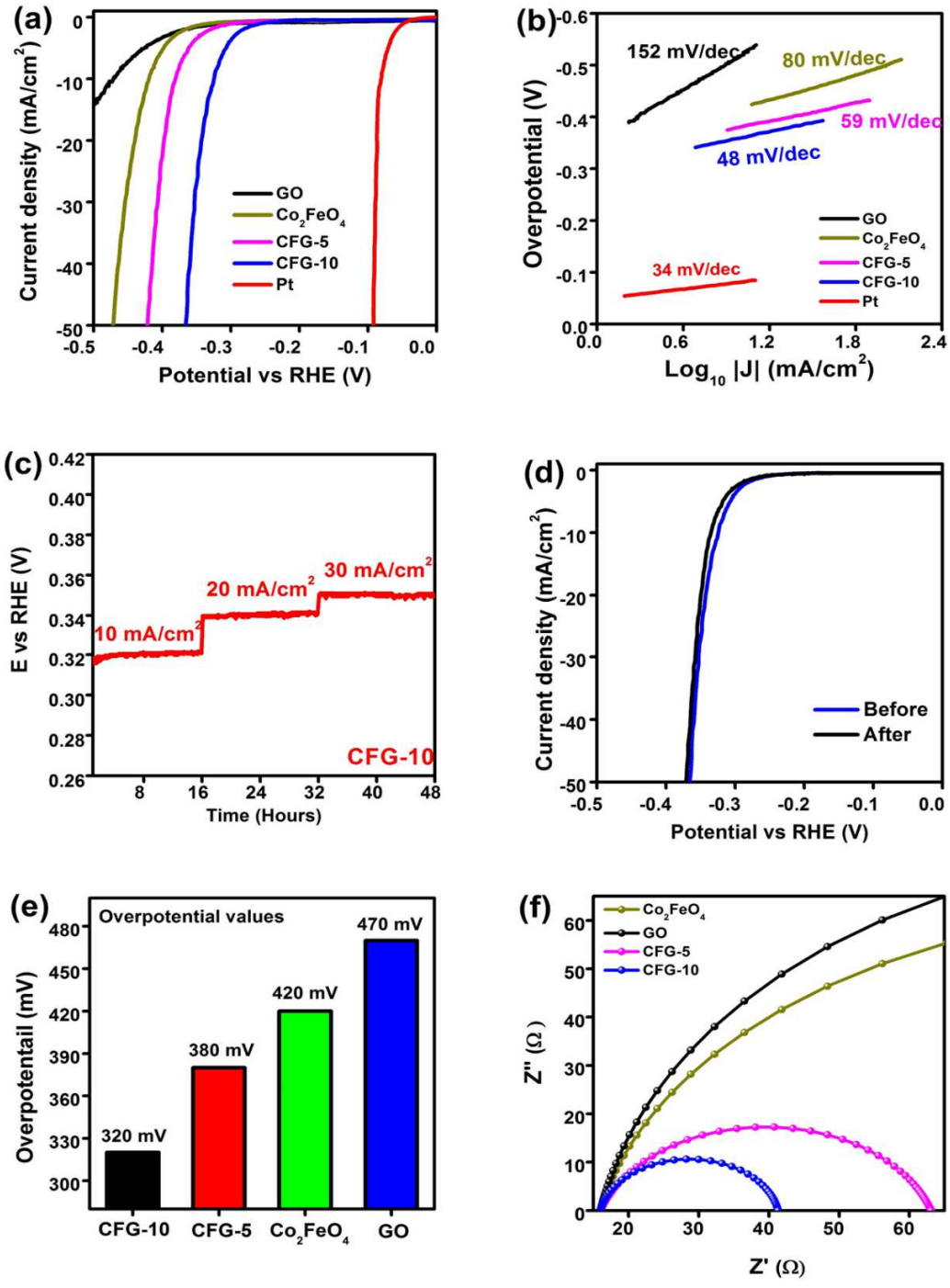
(a)
Current density (mA/cm^2)
Potential vs RHE (V)
GO
Co_2FeO_4
CFG-5
CFG-10
Pt
(b)
Overpotential (V)
Log_{10} |J| (mA/cm^2)
152 mV/dec
80 mV/dec
59 mV/dec
48 mV/dec
34 mV/dec
(c)
E vs RHE (V)
Time (Hours)
10 mA/cm^2
20 mA/cm^2
30 mA/cm^2
CFG-10
(d)
Current density (mA/cm^2)
Potential vs RHE (V)
Before
After
(e)
Overpotential values
Overpotentail (mV)
320 mV
380 mV
420 mV
470 mV
CFG-10
CFG-5
Co_2FeO_4
GO
(f)
Co_2FeO_4
GO
CFG-5
CFG-10
Z'' (Ω)
Z' (Ω)

Table 1. Electrochemical features of various electrocatalysts for OER, HER and ORR

Catalyst	Calculation by LSV						Calculation by EIS				Calculation by CV	
	OER		HER		ORR		OER		HER		Double Layer Capacitance	Electrochemical Active Surface Area
	Tafel Slope	Overpotential at 20 mA/cm^2	Tafel Slope	Overpotential at 10 mA/cm^2	Onset Potential	Half wave Potential	Charge Transfer Resistance	Double Layer Capacitance	Charge Transfer Resistance	Double Layer Capacitance		
	B	η	*B*	η	*V vs RHE*	*V vs RHE*	R_{ct}	CPE_{dl}	R_{ct}	CPE_{dl}	C_{dl}	*ECSA*
	mV/dec	*mV*	*mV/dec*	*mV*	*V*	*V*	Ω	*mF*	Ω	*mF*	$\mu F/cm^2$	cm^2
GO	105	350	152	470	0.74	0.59	1020	0.32	1230	0.29	3.1	77.5
Pristine Co_2FeO_4	68	290	80	420	0.66	0.58	780.8	1.31	960.5	1.45	7.3	182.5
CFG-5	56	260	59	380	0.69	0.56	395	2.72	380.7	2.10	16.6	415
CFG-10	51	240	48	320	0.72	0.60	58.5	5.24	64.8	4.95	23.2	580

Supporting Information

Co_2FeO_4@rGO composite: Towards trifunctional water splitting in alkaline media

Abdul Hanan[a], Dong Shu[a], Umair Aftab[b], Dianxue Cao[a*], Abdul Jaleel Laghari[b], Muhammad Yameen Solangi[b], Muhammad Ishaque Abro[b], Ayman Nafady[e], Brigitte Vigolo[d], Aneela Tahira[c], Zafar Hussain Ibupoto[c]*

[a]Key Laboratory of Superlight Material and Surface Technology, Ministry of Education, College of Materials Science and Chemical Engineering, Harbin Engineering University, PR China.

[b]Department of Metallurgy and Materials Engineering, Mehran University of Engineering and Technology, 76080, jamshoro, Pakistan.

[c]Dr. M.A Kazi Institute of Chemistry University of Sindh Jamshoro, 76080, Sindh Pakistan

[d]Université de Lorraine, CNRS, IJL, F-54000 Nancy, France

[e]Department of Chemistry, College of Science, King Saud University, Riyadh 11451, Saudi Arabia

*Corresponding authors: Dianxue Cao and Zafar Hussain Ibupoto

Email : caodianxue@hrbeu.edu.cn zaffar.ibhupoto@usindh.edu.pk

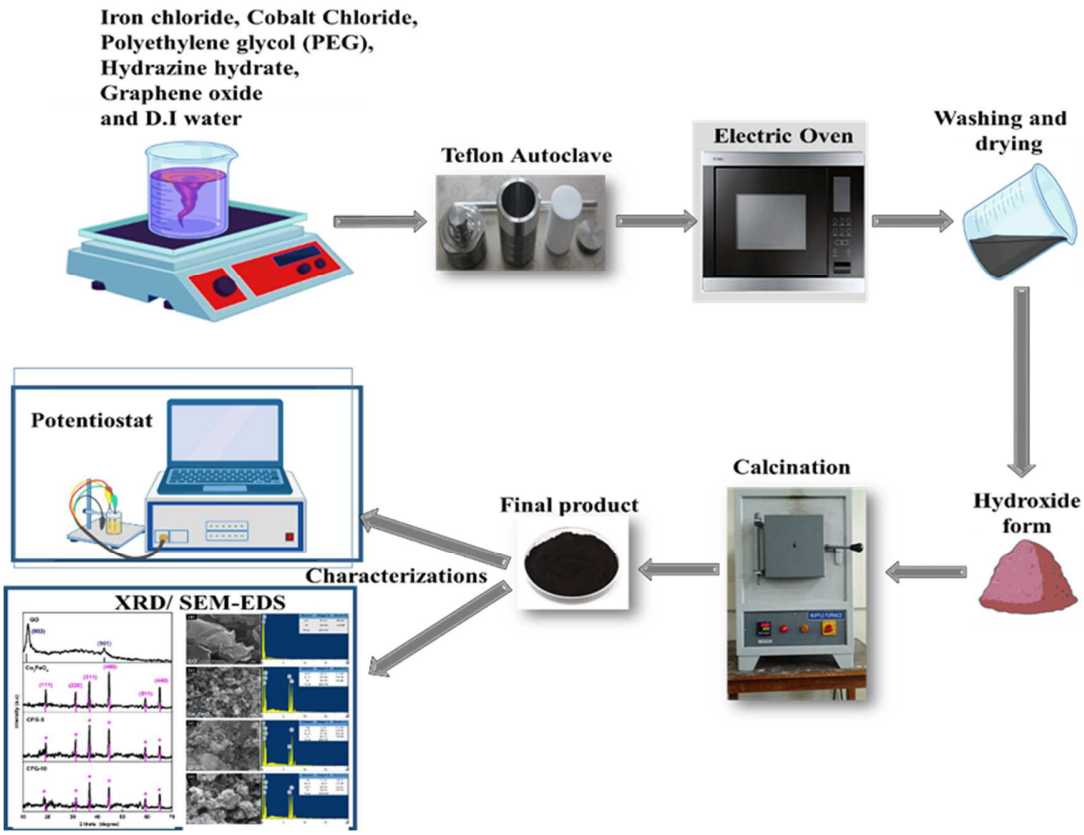

Scheme 1: Synthesis process of Co_2FeO_4@rGO composite, structural characterization and electrochemical set up for multifunctional surface properties

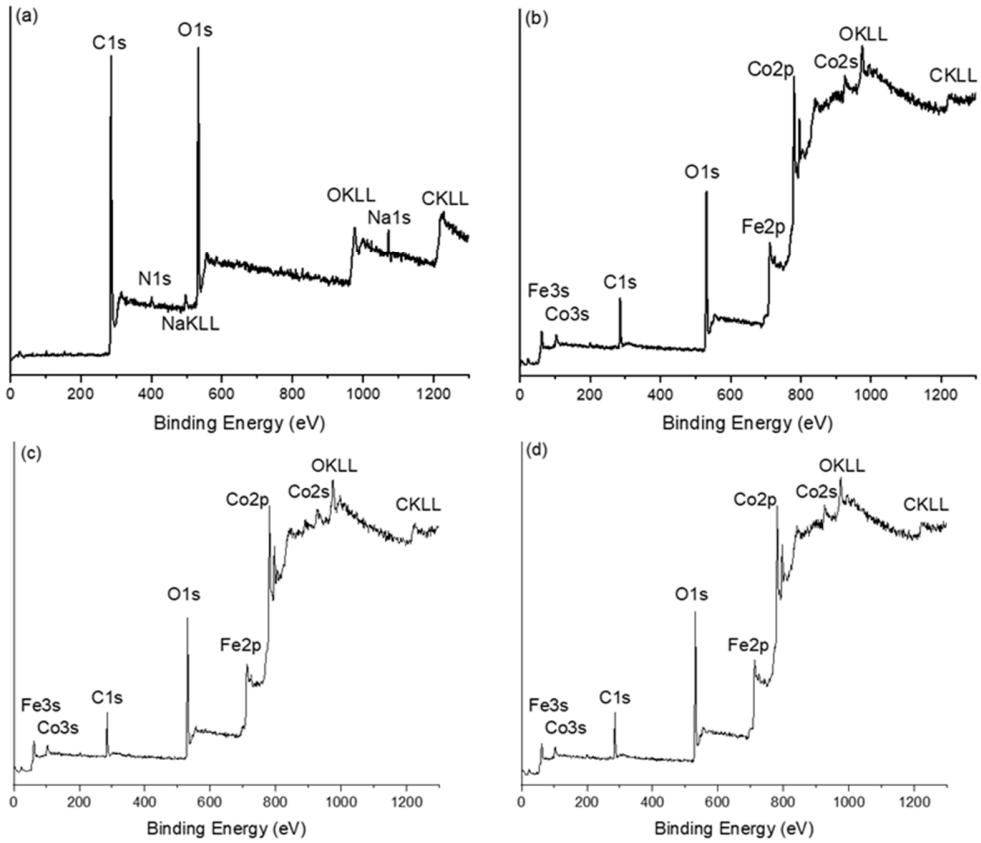

Fig S1(a) XPS Survey scan (a) GO, (b) Co_2FeO_4, (c) CFG-5, (d) CFG-10

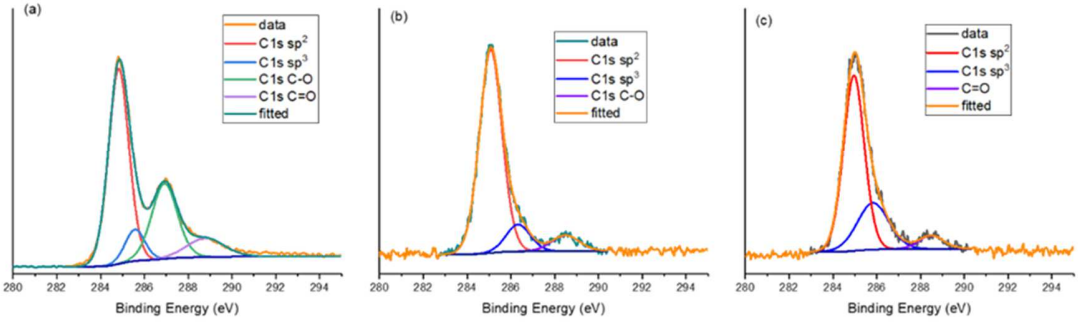

Fig. S1(b) XPS C1s (a) GO, (b) CFG-5, (c) CFG-10

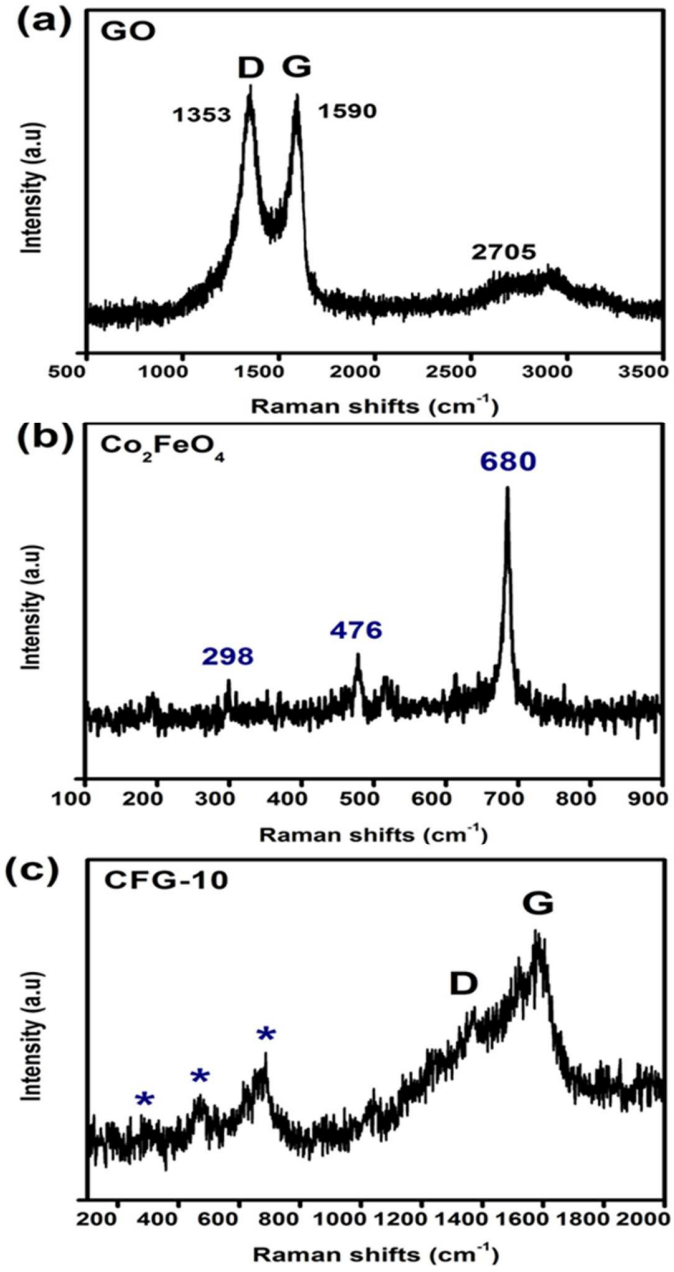

Fig. S2 Raman spectroscopy of various nanostructures (a) GO (b) Co_2FeO_4 and (c) CFG-10 composite

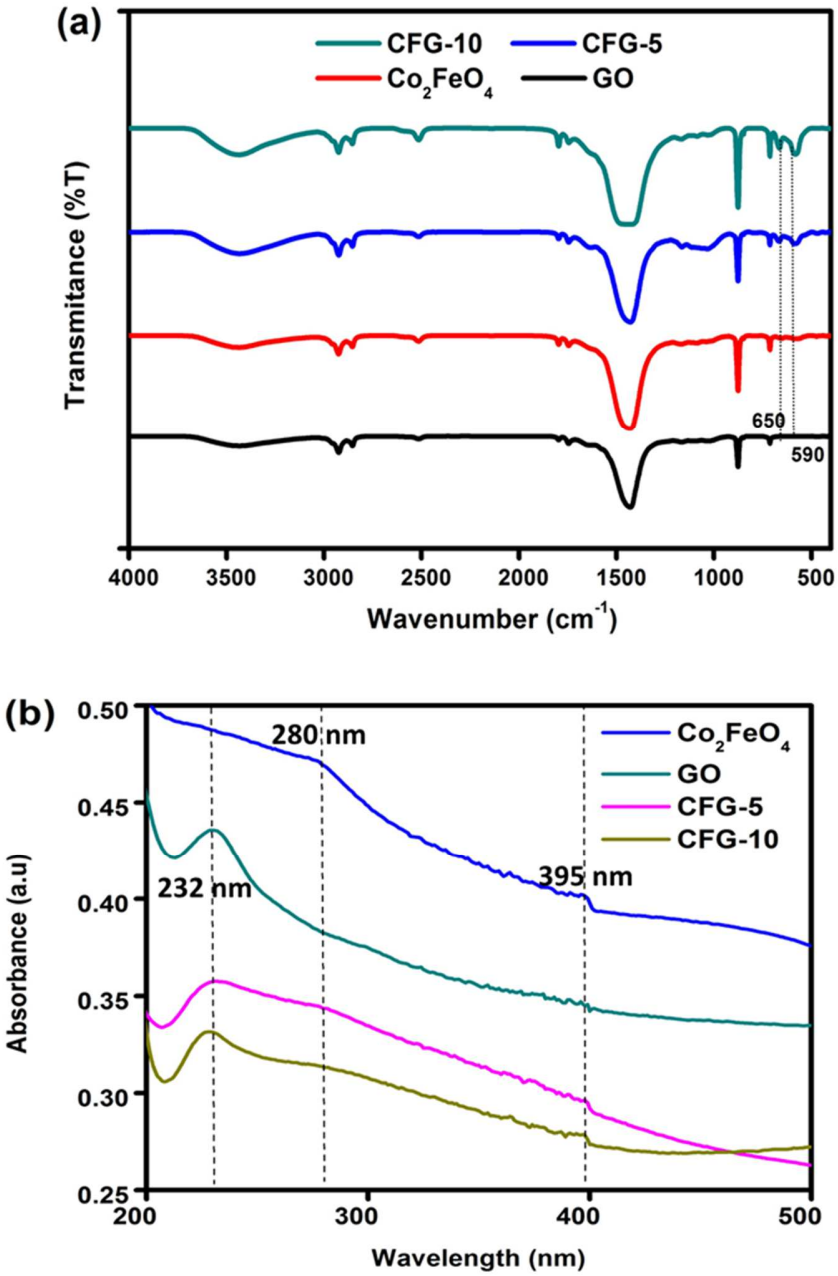

Fig. S3 (a) FTIR spectra of various nanostructures GO, Co_2FeO_4, CFG-5 and CFG-10 (b) UV-vis analysis of as synthesized nanostructures

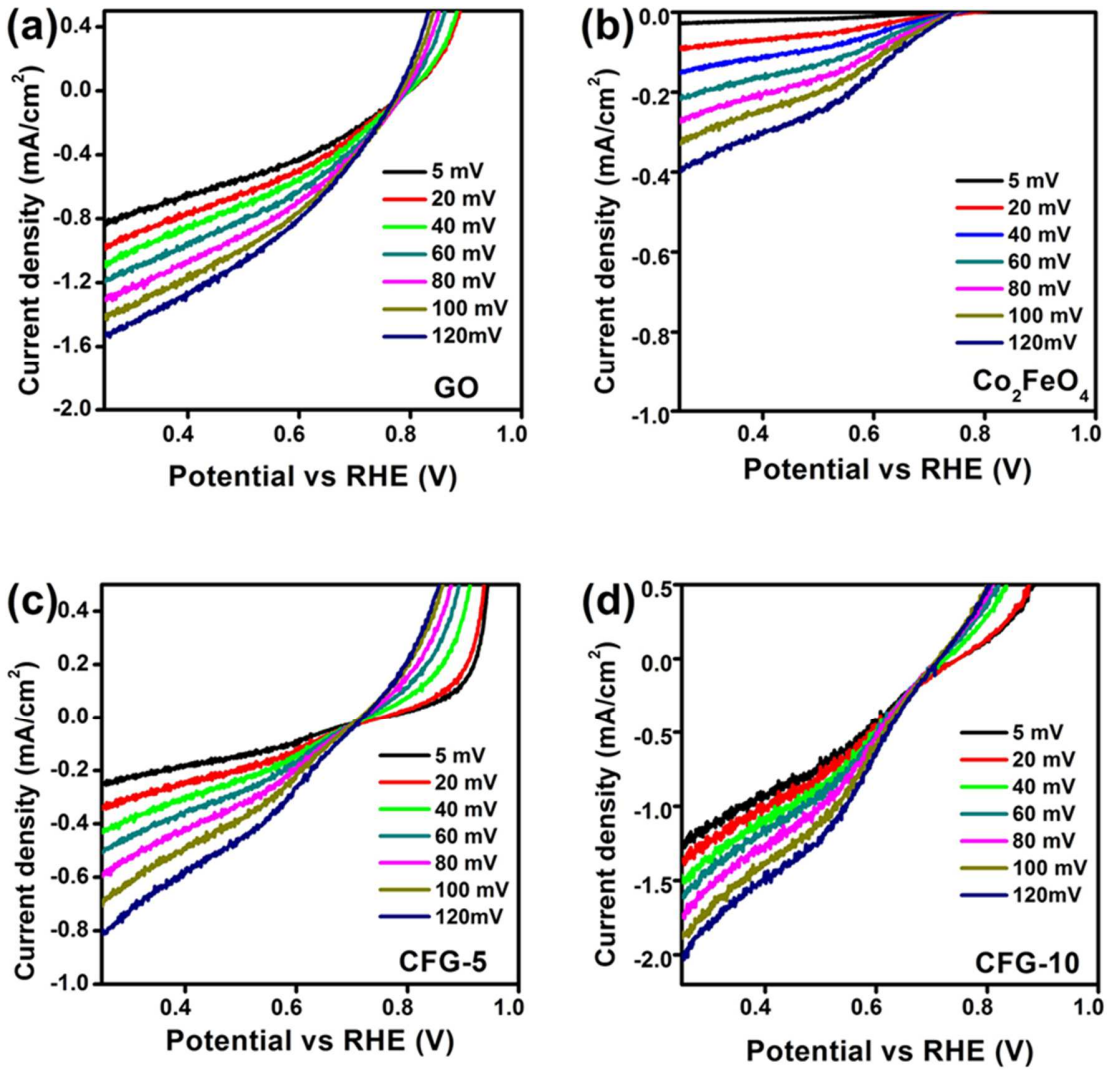

Fig. S4 Corresponding ORR activity of various nanostructures with varying scan rates at zero rotation speed

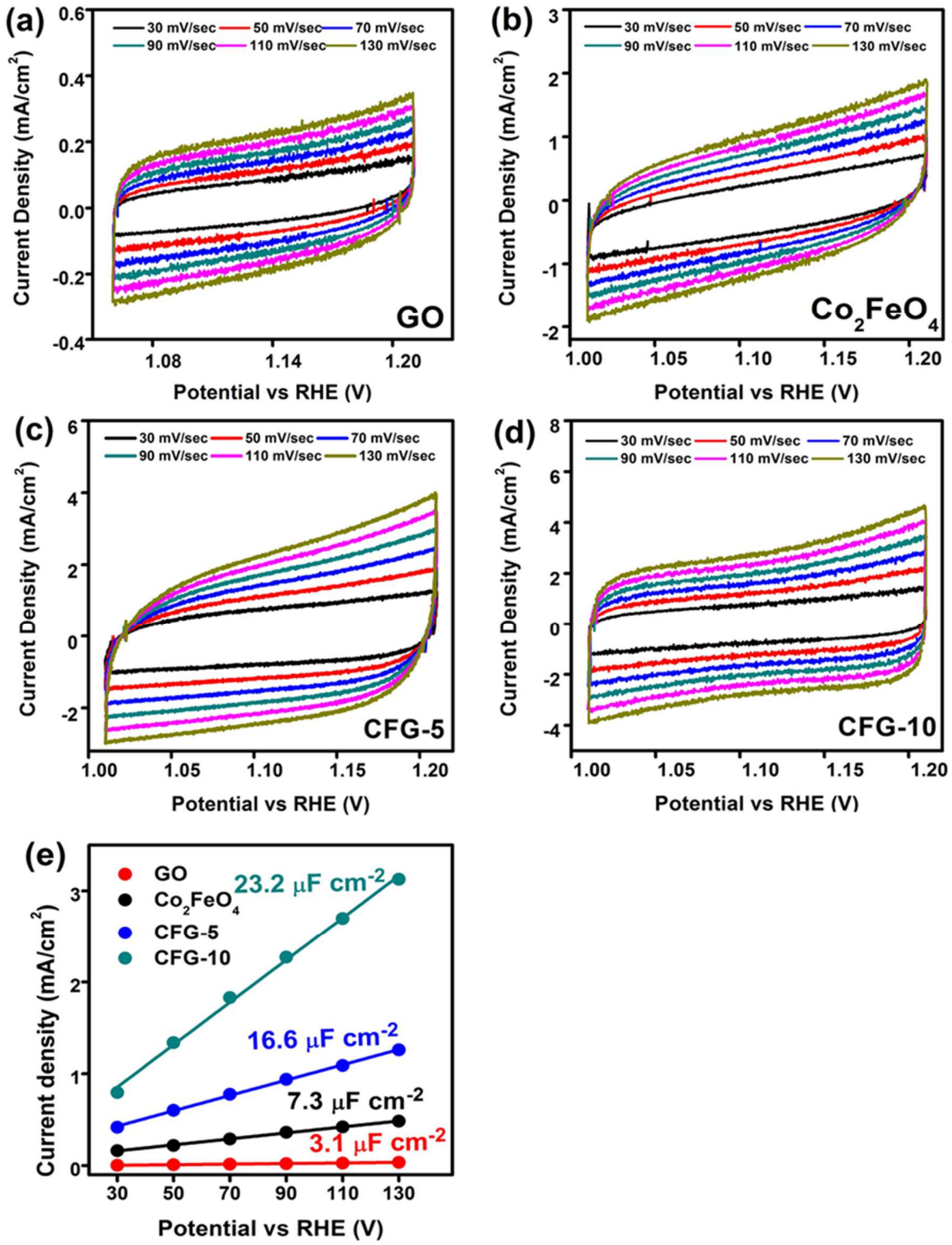

Fig. S5 CV curves of various nanostructures to determine corresponding double layer capacitance values (a) GO, (b) Co_2FeO_4, (c) CFG-5 and (d) CFG-10

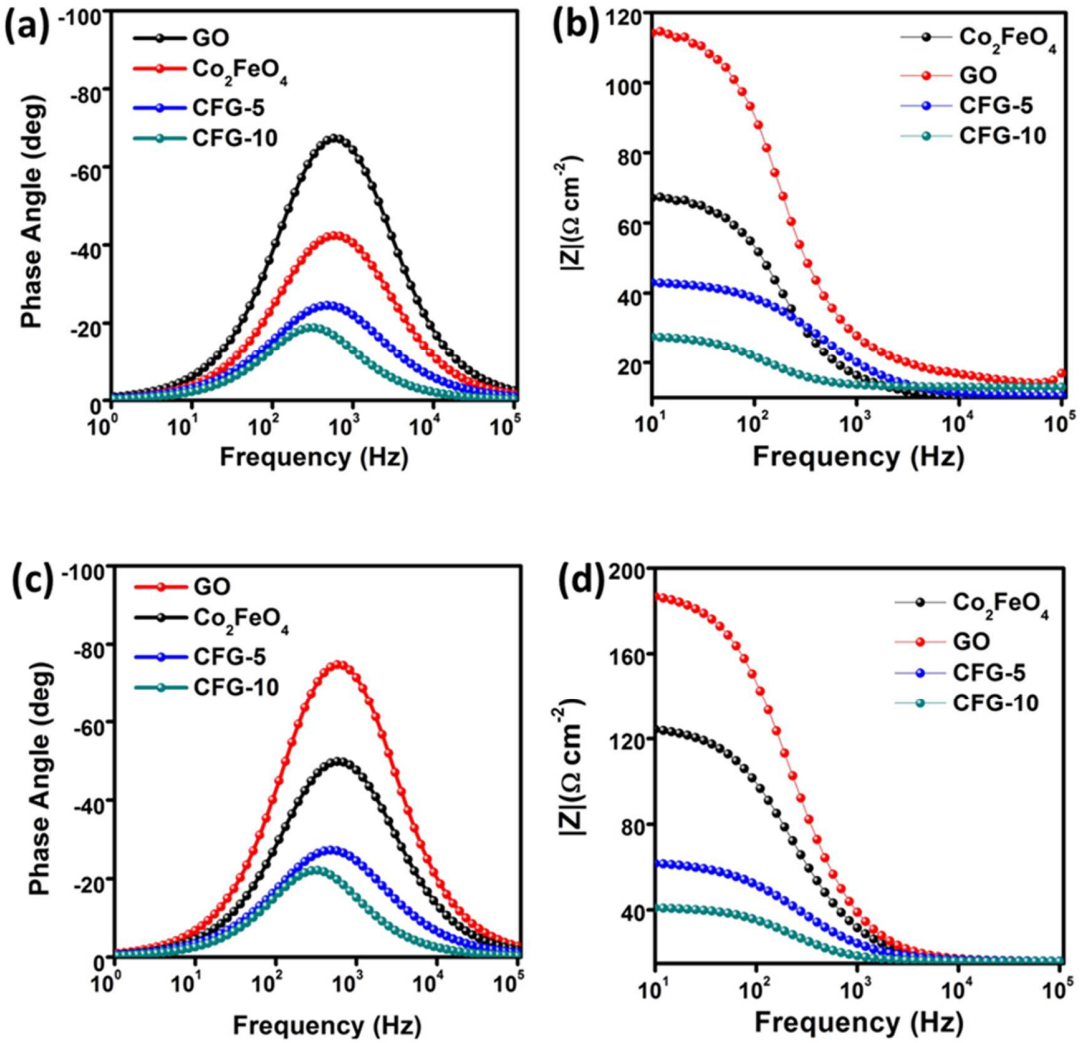

Fig. S6 Corresponding Bode plots (I and II) from EIS data (a and b) for OER analysis (c and d) for HER activity as well

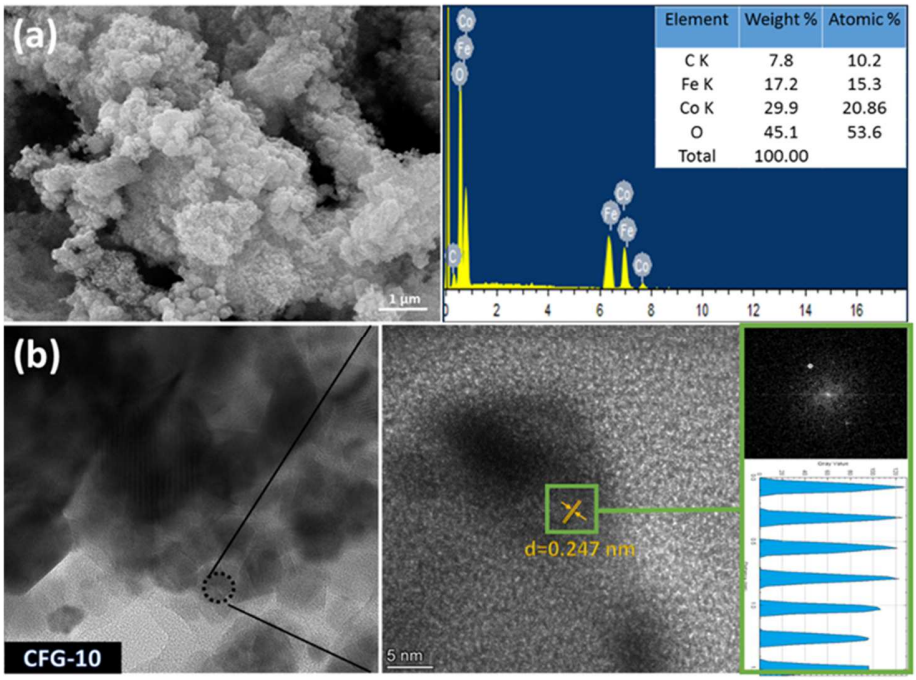

Fig. S7 After chronopotentiometry for OER the Co_2FeO_4@rGO like CFG-10 composite was analyzed (a) SEM/EDS image (b) HRTEM image with relevant FFT image and lattice fringes information

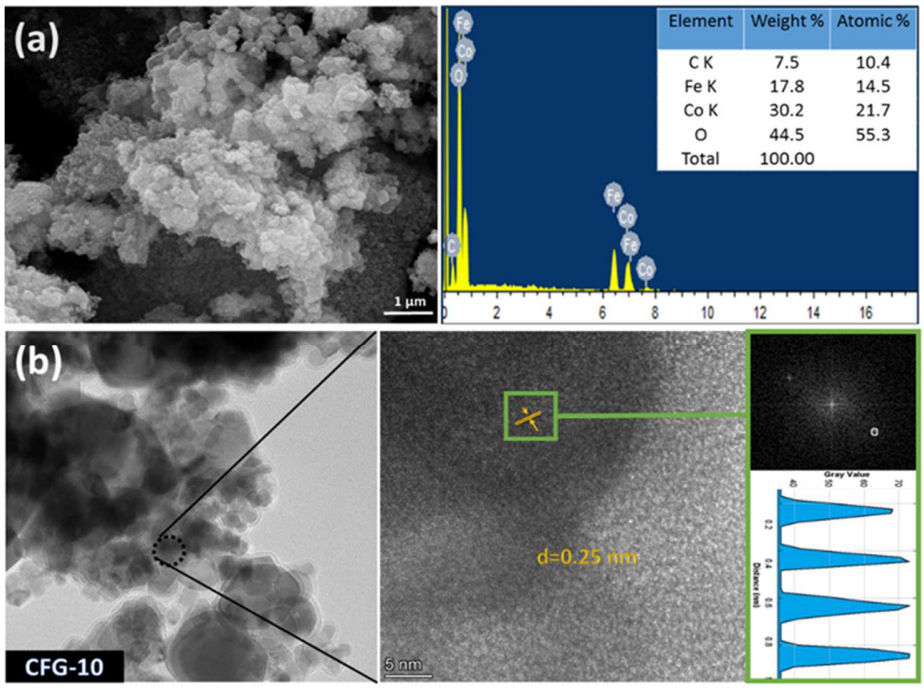

Fig. S8 After chronopotentiometry for HER the Co_2FeO_4@rGO like CFG-10 composite was analyzed (a) SEM/EDS image (b) HRTEM image with relevant FFT image and lattice fringes information

Table S1. Comparative study of previous reported electrocatalysts for HER and current work.

Electrocatalyst	Electrolyte	Current density	Overpotential	Tafel slope	Reference
CFG-10	1M KOH	10 mA/cm^2	320 mV	48 mV/dec	**This work**
FeO_x-NBs	0.5M KOH	50 mA/cm^2	450 mV	85 mV/dec	[1]
$NiFe_2O$	4.24M KOH	10 mA/cm^2	350 mV	120 mV/dec	[2]
Ni_xSe/GO	1M KOH	30 mA/cm^2	320 mV	91 mV/dec	[3]
Fe-NiS/$Ni(OH)_2$	1M KOH	10 mA/cm^2	350 mV	95 mV/dec	[4]
Co_3O_4/Ppy/C	1M KOH	10 mA/cm^2	340 mV	87 mV/dec	[5]
Co@NGr	1M KOH	10 mA/cm^2	340 mV	146 mV/dec	[6]
$Co_{1-x}Fe_xP_3$	1M KOH	50 mA/cm^2	330 mV	65 mV/dec	[7]

Table S2. Comparative study of previous reported electrocatalysts for OER and current work

Electrocatalyst	Electrolyte	Current density	Overpotential	Tafel slope	Reference
CFG-10	1M KOH	20 mA/cm^2	240 mV	51 mV/dec	**This work**
Co_3O_4@ZIF-67	1M KOH	10 mA/cm^2	330 mV	73 mV/dec	[8]
Graphene-Co_3O_4	1M KOH	10 mA/cm^2	313 mV	49 mV/dec	[9]
CoP/rGO	1M KOH	10 mA/cm^2	340 mV	50 mV/dec	[10]
Co-TiO_2	1M KOH	50 mA/cm^2	300 mV	72 mV/dec	[11]
FeCoNiP	1M KOH	10 mA/cm^2	350 mV	60 mV/dec	[12]
Ni–Fe Oxide	1M KOH	60 mA/cm^2	290 mV	58 mV/dec	[13]
FeNiS2 NS/rGO	0.1M KOH	10 mA/cm^2	270 mV	40 mV/dec	[14]

Table S3. Comparative study of previous reported electrocatalysts for ORR and current work

Electrocatalyst	**Electrolyte**	**Onset potential/ V vs RHE**	**Reference**
CFG-10	1M KOH	0.60	**This work**
MoS_2/N-graphene	0.1M KOH	0.95	[15]
N,S-doped graphene	0.1M KOH	0.875	[16]
N,P-doped graphene frameworks	0.1M KOH	>0.845	[17]
Co_3O_4/rGO	0.1M KOH	0.950	[18]
Co/CoO_x	0.1M KOH	0.2 (vs AgCl)	[19]
rGO/Fe_3O_4	0.1M KOH	0.80	[20]
Fe/Co–CNT	0.1M KOH	0.783	[21]
Pt/AEI/rGO	0.1M KOH	1.05	[22]

Table S4. Comparative study of previous reported Tri-functional and Bi-functional electrocatalysts and current work.

Electrocatalyst	**Electrolyte**	**ORR**	**HER**		**OER**		**Ref.**
		Onset potential/ V vs RHE	**Current density**	**Over-potential**	**Current density**	**Over-potential**	
Co_2FeO_4@GO	1 M KOH	0.60 V	10 mA/cm^2	320 mV	20 mA/cm^2	240 mV	**This work**
D/G-CTs-n	1 M KOH	0.98 V	10 mA/cm^2	320 mV	10 mA/cm^2	420 mV	[23]
Co_3Mo_3N	1 M KOH	0.75 V	10 mA/cm^2	100 mV	10 mA/cm^2	290	[24]
Co/CoO@CoN-C-800	0.1 M KOH	0.78 V	20 mA/cm^2	436 mV	10 mA/cm^2	364 mV	[25]
Defect graphene	0.1 M KOH	0.76 V	10 mA/cm^2	320 mV	10 mA/cm^2	340 mV	[26]
Co0.85Se@NC	1 M KOH	0.81 V	10 mA/cm^2	230 mV	10 mA/cm^2	320 mV	[27]
CoO_x NPs/BNG	0.1 M KOH	0.950 V	10 mA/cm^2	295 mV	-	-	[28]
$YBaCo_4O_{7+d}$	0.1 M KOH	0.82 V	1.18 mA/cm^2	400 mV	-	-	[29]
$NiCo_{Ss}$	1 M KOH	-	20 mA/cm^2	234 mV	10 mA/cm^2	168 mV	[30]
VoB-Co_3O_4/NF	1 M KOH	-	50 mA/cm^2	184 mV	50 mA/cm^2	315 mV	[31]
Co_3O_4 (3)/lsm-TiO_2	1 M KOH	0.84 V	-	-	10 mA/cm^2	348 mV	[32]
Co–N/S/rGO	0.1 M KOH	0.85 V	-	-	10 mA/cm^2	320 mV	[33]

References

[1] Babar, N.-U.-A., Y.F. Joya, H. Khalil, F. Hussain and K.S. Joya, Thin-film iron-oxide nanobeads as bifunctional electrocatalyst for high activity overall water splitting. International Journal of Hydrogen Energy. 46(2021). 7885-7902.
[2] Faid, A.Y., A.O. Barnett, F. Seland and S. Sunde, Optimized Nickel-Cobalt and Nickel-Iron Oxide Catalysts for the Hydrogen Evolution Reaction in Alkaline Water Electrolysis. Journal of The Electrochemical Society. 166(2019). F519-F533.
[3] Liu, G., C. Shuai, Z. Mo, R. Guo, N. Liu, X. Niu, Q. Dong, J. Wang, Q. Gao, Y. Chen, and W. Liu, The one-pot synthesis of porous Ni0.85Se nanospheres on graphene as an efficient and durable electrocatalyst for overall water splitting. New Journal of Chemistry. 44(2020). 17313-17322.
[4] Kandiel, T.A., Iron-incorporated NiS/Ni(OH)2 composite as an efficient electrocatalyst for hydrogen evolution reaction from water in a neutral medium. Applied Catalysis A: General. 586(2019). 117226.
[5] Jayaseelan, S.S., N. Bhuvanendran, Q. Xu and H. Su, Co3O4 nanoparticles decorated Polypyrrole/carbon nanocomposite as efficient bi-functional electrocatalyst for electrochemical water splitting. International Journal of Hydrogen Energy. 45(2020). 4587-4595.
[6] Bhadu, G.R., B. Parmar, P. Patel, J.C. Chaudhari and E. Suresh, Controlled assembly of cobalt embedded N-doped graphene nanosheets (Co@NGr) by pyrolysis of a mixed ligand Co(ii) MOF as a sacrificial template for high-performance electrocatalysts. RSC Advances. 11(2021). 21179-21188.
[7] Lin, L., Q. Fu, Y. Han, J. Wang, X. Zhang, Y. Zhang, C. Hu, Z. Liu, Y. Sui, and X. Wang, Fe doped skutterudite-type CoP3 nanoneedles as efficient electrocatalysts for hydrogen and oxygen evolution in alkaline media. Journal of Alloys and Compounds. 808(2019). 151767.
[8] Liu, X., H. Liu, G. He, Y. Zhu, J. Xiao, and L. Han, Borate Anion Dopant Inducing Oxygen Vacancies over Co3O4 Nanocages for Enhanced Oxygen Evolution. Catalysts. 11(2021). 659.
[9] Zhao, Y., S. Chen, B. Sun, D. Su, X. Huang, H. Liu, Y. Yan, K. Sun, and G. Wang, Graphene-Co(3)O(4) nanocomposite as electrocatalyst with high performance for oxygen evolution reaction. Sci Rep. 5(2015). 7629.
[10] Jiao, L., Y.X. Zhou and H.L. Jiang, Metal-organic framework-based CoP/reduced graphene oxide: high-performance bifunctional electrocatalyst for overall water splitting. Chem Sci. 7(2016). 1690-1695.
[11] Liu, C., J. Qian, Y. Ye, H. Zhou, C.-J. Sun, C. Sheehan, Z. Zhang, G. Wan, Y.-S. Liu, J. Guo, S. Li, H. Shin, S. Hwang, T.B. Gunnoe, W.A. Goddard, and S. Zhang, Oxygen evolution reaction over catalytic single-site Co in a well-defined brookite TiO2 nanorod surface. Nature Catalysis. 4(2021). 36-45.
[12] Xu, J., J. Li, D. Xiong, B. Zhang, Y. Liu, K.-H. Wu, I. Amorim, W. Li, and L. Liu, Trends in activity for the oxygen evolution reaction on transition metal (M = Fe, Co, Ni) phosphide pre-catalysts. Chemical science. 9(2018). 3470-3476.
[13] Yu, M., G. Moon, E. Bill and H. Tüysüz, Optimizing Ni–Fe Oxide Electrocatalysts for Oxygen Evolution Reaction by Using Hard Templating as a Toolbox. ACS Applied Energy Materials. 2(2019). 1199-1209.
[14] Jiang, J., S. Lu, W.-K. Wang, G.-X. Huang, B.-C. Huang, F. Zhang, Y.-J. Zhang, and H.-Q. Yu, Ultrahigh electrocatalytic oxygen evolution by iron-nickel sulfide nanosheets/reduced graphene oxide nanohybrids with an optimized autoxidation process. Nano Energy. 43(2018). 300-309.
[15] Du, C., H. Huang, X. Feng, S. Wu and W. Song, Confining MoS2 nanodots in 3D porous nitrogen-doped graphene with amendable ORR performance. Journal of Materials Chemistry A. 3(2015). 7616-7622.
[16] Pan, F., Y. Duan, X. Zhang and J. Zhang, A Facile Synthesis of Nitrogen/Sulfur Co-Doped Graphene for the Oxygen Reduction Reaction. ChemCatChem. 8(2016). 163-170.

[17] Chai, G.-L., K. Qiu, M. Qiao, M.-M. Titirici, C. Shang, and Z. Guo, Active sites engineering leads to exceptional ORR and OER bifunctionality in P,N Co-doped graphene frameworks. Energy & Environmental Science. 10(2017). 1186-1195.
[18] Goswami, C., K.K. Hazarika and P. Bharali, Transition metal oxide nanocatalysts for oxygen reduction reaction. Materials Science for Energy Technologies. 1(2018). 117-128.
[19] Ma, L., S. Chen, Z. Pei, Y. Huang, G. Liang, F. Mo, Q. Yang, J. Su, Y. Gao, J.A. Zapien, and C. Zhi, Single-Site Active Iron-Based Bifunctional Oxygen Catalyst for a Compressible and Rechargeable Zinc–Air Battery. ACS Nano. 12(2018). 1949-1958.
[20] Karunagaran, R., C. Coghlan, T.T. Tung, S. Kabiri, D.N.H. Tran, C.J. Doonan, and D. Losic, Study of iron oxide nanoparticle phases in graphene aerogels for oxygen reduction reaction. New Journal of Chemistry. 41(2017). 15180-15186.
[21] Zhao, Y.M., F.F. Wang, P.J. Wei, G.Q. Yu, S.C. Cui, and J.G. Liu, Cobalt and Iron Oxides Co-supported on Carbon Nanotubes as an Efficient Bifunctional Catalyst for Enhanced Electrocatalytic Activity in Oxygen Reduction and Oxygen Evolution Reactions. ChemistrySelect. 3(2018). 207-213.
[22] Higgins, D., P. Zamani, A. Yu and Z. Chen, The application of graphene and its composites in oxygen reduction electrocatalysis: a perspective and review of recent progress. Energy & Environmental Science. 9(2016). 357-390.
[23] Kong, F., Y. Qiao, C. Zhang, X. Fan, A. Kong, and Y. Shan, Unadulterated carbon as robust multifunctional electrocatalyst for overall water splitting and oxygen transformation. Nano Research. 13(2020). 401-411.
[24] Yuan, Y., S. Adimi, T. Thomas, J. Wang, H. Guo, J. Chen, J.P. Attfield, F.J. DiSalvo, and M. Yang, Co3Mo3N-An efficient multifunctional electrocatalyst. Innovation (N Y). 2(2021). 100096.
[25] Zhang, X., R. Liu, Y. Zang, G. Liu, G. Wang, Y. Zhang, H. Zhang, and H. Zhao, Co/CoO nanoparticles immobilized on Co–N-doped carbon as trifunctional electrocatalysts for oxygen reduction, oxygen evolution and hydrogen evolution reactions. Chemical Communications. 52(2016). 5946-5949.
[26] Jia, Y., L. Zhang, A. Du, G. Gao, J. Chen, X. Yan, C.L. Brown, and X. Yao, Defect Graphene as a Trifunctional Catalyst for Electrochemical Reactions. Adv Mater. 28(2016). 9532-9538.
[27] Meng, T., J. Qin, S. Wang, D. Zhao, B. Mao, and M. Cao, In situ coupling of Co0.85Se and N-doped carbon via one-step selenization of metal–organic frameworks as a trifunctional catalyst for overall water splitting and Zn–air batteries. Journal of Materials Chemistry A. 5(2017). 7001-7014.
[28] Tong, Y., P. Chen, T. Zhou, K. Xu, W. Chu, C. Wu, and Y. Xie, A Bifunctional Hybrid Electrocatalyst for Oxygen Reduction and Evolution: Cobalt Oxide Nanoparticles Strongly Coupled to B,N-Decorated Graphene. Angew Chem Int Ed Engl. 56(2017). 7121-7125.
[29] Kirsanova, M.A., V.D. Okatenko, D.A. Aksyonov, R.P. Forslund, J.T. Mefford, K.J. Stevenson, and Artem M. Abakumov, Bifunctional OER/ORR catalytic activity in the tetrahedral YBaCo4O7.3 oxide. Journal of Materials Chemistry A. 7(2019). 330-341.
[30] Li, M., Z. Xu, Y. Li, J. Wang and Q. Zhong, In situ fabrication of cobalt/nickel sulfides nanohybrid based on various sulfur sources as highly efficient bifunctional electrocatalysts for overall water splitting. Nano Select, (2021).
[31] Yuan, H., S. Wang, Z. Ma, M. Kundu, B. Tang, J. Li, and X. Wang, Oxygen vacancies engineered self-supported B doped Co3O4 nanowires as an efficient multifunctional catalyst for electrochemical water splitting and hydrolysis of sodium borohydride. Chemical Engineering Journal. 404(2021). 126474.

[32] Amer, M.S., M.A. Ghanem, P. Arunachalam, A.M. Al-Mayouf and S.M. Hadadi, Bifunctional Electrocatalyst of Low-Symmetry Mesoporous Titanium Dioxide Modified with Cobalt Oxide for Oxygen Evolution and Reduction Reactions. Catalysts. 9(2019). 836.
[33] Gu, L., X.-L. Sun, J. Zhao, B.-Q. Gong, Z.-L. Bao, H.-L. Jia, M.-Y. Guan, and S.-S. Ma, A highly efficient bifunctional electrocatalyst (ORR/OER) derived from GO functionalized with carbonyl, hydroxyl and epoxy groups for rechargeable zinc–air batteries. New Journal of Chemistry. 45(2021). 6535-6542.